

Signatures of BH seeding on the $M_{\bullet} - \sigma$ relation: Predictions from the BRAHMA simulations

JONATHAN KHO,^{1,2,3} AKLANT KUMAR BHOWMICK,^{1,2,3} PAUL TORREY,^{1,2,3} ALEX M. GARCIA,^{1,2,3} NIUSHA AHVAZI,^{1,2,3}
LAURA BLECHA,⁴ AND MARK VOGELSBERGER⁵

¹University of Virginia 530 McCormick Rd Charlottesville, VA 22904, USA; yja6qa@virginia.edu

²Virginia Institute for Theoretical Astronomy, University of Virginia, Charlottesville, VA 22904, USA

³The NSF-Simons AI Institute for Cosmic Origins, USA

⁴Department of Physics, University of Florida, Gainesville, FL 32611, USA

⁵Department of Physics, Kavli Institute for Astrophysics and Space Research, Massachusetts Institute of Technology, Cambridge, MA 02139, USA

ABSTRACT

The James Webb Space Telescope (JWST) has identified a large population of supermassive (10^6 – $10^8 M_{\odot}$) black holes (BHs) in the early universe ($z \sim 4$ – 7). Current measurements suggest that many of these BHs exhibit higher BH-to-stellar mass ratios than local populations, opening a new window into the earliest stages of BH–galaxy coevolution and offering the potential to place tight constraints on BH seeding and growth in the early universe. In this work, we use the BRAHMA simulations to investigate the impact of BH seeding on the $M_{\bullet} - \sigma$ relation. These simulations adopt heavy $\sim 10^5 M_{\odot}$ seeds and systematically varied BH seeding models, resulting in distinct predictions for seed abundances. We find that different seed models lead to different normalizations of the $M_{\bullet} - \sigma$ relation at higher redshifts ($z > 2$) across all σ , and at low redshift for systems with low σ ($50 \text{ km s}^{-1} \lesssim \sigma \lesssim 80 \text{ km s}^{-1}$). The most lenient seed model also shows negligible evolution in the $M_{\bullet} - \sigma$ relation across redshift, while more restrictive models have substantially lower normalization on the $M_{\bullet} - \sigma$ relation for high σ ($\sim 100 \text{ km s}^{-1}$) at high redshifts, and evolve upward toward the local relation. We demonstrate that the $M_{\bullet} - \sigma$ evolution is a direct consequence of merger-dominated BH growth in low mass galaxies ($\lesssim 10^9 M_{\odot}$) and accretion dominated BH growth in high mass ($\gtrsim 10^9 M_{\odot}$) galaxies. Furthermore, the scatter in the $M_{\bullet} - \sigma$ relation is larger for the more restrictive models due to the inability of many BHs to grow significantly beyond their seed mass.

Keywords: Supermassive black holes(1663) — Scaling relations(2031) — Hydrodynamical simulations(767)

1. INTRODUCTION

It is well established that nearly every massive galaxy contains a supermassive black hole (SMBH) ($M_{\bullet} > 10^6 M_{\odot}$) in its nucleus (Magorrian et al. 1998; Ho 2008; Kormendy & Richstone 1995). These SMBHs have masses that range from $\sim 10^6$ to $10^{10} M_{\odot}$, and are thus distinct from the stellar mass black holes (BH) that are created from the death of a massive star. While the path to forming a stellar mass BH is well-known (Shapiro & Teukolsky 1983; Heger et al. 2023; Laplace et al. 2025), it is still currently unknown how these SMBHs formed (Volonteri 2010; Inayoshi et al. 2020).

Various different seeding channels have been proposed, which are distinguished by forming light, intermediate, and heavy seeds. Light seeds ($M_{\text{seed}} \sim 10^2 M_{\odot}$) are expected to be the remnants of some Population III stars,

which are thought to have been ubiquitous in the early universe (Klessen & Glover 2023). Their low masses, however, have been shown to make growth into the observed 10^9 – $10^{10} M_{\odot}$ BHs very challenging (Milosavljević et al. 2009; Volonteri & Rees 2005; Pezzulli et al. 2016; Klessen & Glover 2023; Smith et al. 2018; Tanaka & Haiman 2009; Jeon et al. 2023; Valiante et al. 2016). Intermediate mass seeds ($M_{\text{seed}} \sim 10^3$ – $10^4 M_{\odot}$) may be formed via stellar collisions or hierarchical BH mergers in a dense nuclear star cluster (Portegies Zwart & McMillan 2002; Arca Sedda et al. 2023; Reinoso et al. 2023; Fragione et al. 2022). Heavy seeds ($M_{\text{seed}} \sim 10^4$ – $10^5 M_{\odot}$), thought to be formed through the direct collapse of a cloud of gas, are much more difficult to form but have the benefit of being able to grow more easily due to their larger initial seed mass. In particular,

producing a heavy seed requires environmental conditions like low metallicities or a critical Lyman-Werner flux which suggests that they are too rare to explain the number densities of either the high- z AGN or the local SMBH populations (Regan & Volonteri 2024).

Beyond having unknown origins, these SMBHs also curiously have very tight scaling relations with properties of their host galaxies (see Kormendy & Ho 2013, for a review). Specifically, in the local Universe, we find that the measured masses (M_{\bullet}) of SMBHs strongly correlate with the stellar mass (M_{\star}) and stellar velocity dispersion of the host galaxy bulge (σ) (Reines & Volonteri 2015; Magorrian et al. 1998; Marconi & Hunt 2003; Gebhardt et al. 2000; Ferrarese & Merritt 2000). Both of these correlations are remarkable because the spatial extent of a galaxy ($\sim\text{kpc}$) far exceeds the region directly influenced by the SMBH’s gravity ($\sim\text{pc}$). These correlations could suggest a ‘coupled’ evolution between BHs and their host galaxies, or they might arise as a statistical consequence of the concurrent growth of black holes and galaxies through hierarchical structure formation. The coupled evolution of BHs and host galaxies as a consequence of AGN feedback has been studied at length in simulations, and suggests that AGN activity may play an important role in driving these tight correlations (e.g. Habouzit et al. 2019; Terrazas et al. 2020; Di Matteo et al. 2005).

In the new era of the James Webb Space Telescope, our understanding of both BH seeding models and BH-galaxy scaling relations is being transformed as a population of high- z ($z = 4 - 7$) broad line AGN (BLAGN) with masses of $M_{\bullet} \sim 10^{6-8}M_{\odot}$ has been discovered (Maiolino et al. 2024a; Natarajan et al. 2024; Bogdán et al. 2024; Greene et al. 2024; Lin et al. 2024; Harikane et al. 2023; Kovács et al. 2024). The discovery of these AGN allows us to probe galaxy scaling relations at high redshift for the first time. This emerging population of BHs appears to be 10 – 100 times more massive than what would be predicted by local stellar mass scaling relations, suggesting that the $M_{\bullet} - M_{\star}$ relation may evolve with redshift (Pacucci et al. 2023; Pacucci & Loeb 2024; Maiolino et al. 2024b; Sun et al. 2025; Furtak et al. 2024). The ubiquity of these JWST BLAGN (Harikane et al. 2023; Akins et al. 2024; Kokorev et al. 2024; Greene et al. 2024) that appear overmassive suggests that heavy BH seeds may not be as rare as previously thought, as overmassive BHs are one of the key signatures of heavy seeds (Agarwal et al. 2013; Natarajan et al. 2017; Visbal & Haiman 2018; Scoggins et al. 2023; Natarajan et al. 2024; Scoggins & Haiman 2024). While there does exist some debate as to whether a subpopulation of these BLAGN (dubbed little red dots (LRDs) due to their

compact morphology and steep red rest-frame continuum) are truly reddened or dust-obscured AGN as opposed to dusty starburst galaxies (Akins et al. 2023; Ananna et al. 2024; Pérez-González et al. 2024; Williams et al. 2024), more recent work has seemed to strongly favor the AGN hypothesis, though several different AGN interpretations abound (Rusakov et al. 2025; Naidu et al. 2025; Juodžbalis et al. 2025; Kido et al. 2025). Nonetheless, these BH masses taken at face value pose strong constraints for BH seeding and growth (see section 11 of Stark et al. 2025, for a brief review).

Interestingly, Bhowmick et al. (2024b,c) found that BHs seeded both as extrapolated seed descendants of light ($M_{\text{seed}} = 10^3M_{\odot}$) seeds and directly as heavy ($M_{\text{seed}} = 10^5M_{\odot}$) seeds were over massive compared to the local $M_{\bullet} - M_{\star}$ relation at $z = 4 - 7$, in good agreement with the high- z JWST AGN that have been discovered. Bhowmick et al. (2024c) also found that the $M_{\bullet} - M_{\star}$ relation can provide strong constraints on BH seeding, since an overmassive $M_{\bullet} - M_{\star}$ relation at high- z suggests a more efficient production of heavy seeds than is typically assumed possible. Furthermore, while both Maiolino et al. (2024b) and Juodžbalis et al. (2025) found their sample of AGN to be over massive on the $M_{\bullet} - M_{\star}$ plane, these same BHs were largely consistent with the local $M_{\bullet} - \sigma$ relation, leading to questions about which scaling relations evolve over cosmic time and why. Since Bhowmick et al. (2024c) found that signatures of BH seeding were found in the $M_{\bullet} - M_{\star}$ relation due to different regimes of merger-driven versus accretion-driven BH growth, it is natural to search for these signatures in the $M_{\bullet} - \sigma$ relation as well.

Volonteri & Natarajan (2009) used a Semi-Analytic model (SAM) to investigate potential signatures of black hole seeding in the $M_{\bullet} - \sigma$ relation. They found that massive seeds tend to form over massive relative to the local $M_{\bullet} - \sigma$ relation, and track horizontally onto it by growing in σ , whereas light seeds form under massive relative to the local relation and track upward by growing the central BH mass while leaving σ relatively unchanged. However, in their model for BH growth, they assumed the local $M_{\bullet} - \sigma$ relation to be constant across redshift, and were thus unable to form conclusions about a $M_{\bullet} - \sigma$ redshift evolution. While SAMs are useful, cheap models that can provide insights into the questions of BH seeding and its impact on galaxy scaling relations, cosmological simulations are necessary as they provide a more reliable and self-consistent method of tracking the seeding conditions, growth, and (co)-evolution of BHs and their host galaxies.

In light of previous work, our goal here is to search for signatures of BH seeding in the BRAHMA simulations by

analyzing the slope, scatter, and possible redshift evolution of the $M_{\bullet} - \sigma$ relation for different BH seed models. Although other studies have examined the impact of different BH seeding prescriptions on (heavy) direct-collapse BH formation sites (e.g. [Dunn et al. 2018](#); [Luo et al. 2020](#)), and there have been many SAM studies examining the effects of different BH seeding prescriptions (e.g. [Volonteri & Natarajan 2009](#); [Spinoso et al. 2023](#); [Evans et al. 2025](#)), we are unaware of any other study thus far examining the effect of varying BH seeding prescriptions on the $M_{\bullet} - \sigma$ relation with cosmological simulations. The BRAHMA simulations are thus ideal for this work because they provide unique seeding criteria for heavy BH seeds that have not been implemented in other hydrodynamic simulations, and which have been studied in depth with cosmological zoom simulations prior to their implementation in these full volume simulations ([Bhowmick et al. 2021, 2022a,b](#)).

The structure of this paper is as follows: we describe the BRAHMA simulations and our methods in section 2, present our results in section 3, comment on JWST observations and uncertainties in our results in section 4 and provide concluding thoughts in section 5.

2. METHODS

The BRAHMA simulations were run using the AREPO gravity + magnetohydrodynamic (MHD) solver ([Springel 2010](#); [Pakmor et al. 2011, 2016](#); [Weinberger et al. 2020](#)). The gravity solver uses the Particle Mesh Tree ([Barnes & Hut 1986](#)) and the evolution of the gas is described by the ideal MHD equations solved over a dynamic unstructured grid generated via a Voronoi tessellation of the domain. All the simulations are characterized by the Planck Collaboration XIII (2016) cosmology i.e. $\Omega_{\Lambda} = 0.6911$, $\Omega_{\text{m}} = 0.3089$, $\Omega_{\text{b}} = 0.0486$, $H_0 = 67.76 \text{ km s}^{-1} \text{ Mpc}^{-1}$, $\sigma_8 = 0.8159$, $n_s = 0.9667$. Halos are identified using the Friends-of-Friends (FOF) algorithm ([Davis et al. 1985](#)) with a linking length of 0.2 times the mean particle separation. Subhalos are identified using the SUBFIND ([Springel et al. 2001](#)) algorithm. The initial conditions were created using the MUSIC algorithm at $z = 127$ ([Hahn & Abel 2011](#)). The simulations are run in a comoving volume of $[18 \text{ Mpc}]^3$ with 512 dark matter (DM) particles. The DM mass resolution is $1.5 \times 10^6 M_{\odot}$, and the target baryon mass resolution is $2.4 \times 10^5 M_{\odot}$.

2.1. Galaxy formation model

Aside from BH seeding, the BRAHMA simulations adopt all of the features of the IllustrisTNG model (hereafter TNG; [Pillepich et al. 2018a](#); [Weinberger et al. 2018](#)), which itself is based on the Illustris model ([Vogels-](#)

[berger et al. 2013](#); [Torrey et al. 2014](#)). Radiative cooling includes the contributions from primordial species (H, H⁺, He, He⁺, He⁺⁺ according to [Katz et al. 1996](#)) and metals ([Wiersma et al. 2009](#)). Metal cooling rates are interpolated from tables calculated in the presence of a spatially uniform, time-dependent UV background. As gas cools and condenses, star formation occurs when gas densities exceed 0.13 cm^{-3} . Star-forming gas cells (i.e. those exceeding the star formation density threshold) are considered to represent a multi-phase ISM via a subgrid, effective equation of state ([Springel & Hernquist 2003](#)). Star particles represent full stellar populations with each particle being characterized by a single stellar age and metallicity. The initial stellar mass function is taken from [Chabrier \(2003\)](#), and the stellar evolution model is based on [Vogelsberger et al. \(2013\)](#) with modifications for TNG described in [Pillepich et al. \(2018a\)](#). Stellar chemical enrichment is modeled by following the evolution of (H, He, C, N, O, Ne, Mg, Si, Fe). Supernova feedback is modeled as a galactic-scale wind depositing mass, momentum, and metals to surrounding gas cells.

BHs in our simulations grow through two channels: accretion and mergers. Accretion is modeled with an Eddington-limited Bondi-Hoyle model ([Bondi & Hoyle 1944](#); [Bondi 1952](#)). The Eddington limit and BH bolometric luminosities are calculated with an assumed radiative efficiency of $\epsilon = 0.2$. AGN feedback is modeled as one of two modes: ‘kinetic’ or ‘thermal’. Thermal feedback is implemented for high Eddington ratios, wherein a fraction of the radiated luminosity is deposited in neighboring gas cells. Kinetic feedback is used for low Eddington ratios, wherein kinetic energy is injected to the gas in random directions at irregular time intervals. In our simulations, a BH merger occurs when at least one BH lies within the ‘neighbor search radius’ of the other. Furthermore, BHs are re-positioned to the nearest potential minimum within 1000 nearest gas cells at each time step to avoid spurious gravitational kicks from massive DM particles, which are ~ 10 times more massive than our BH seeds. This means every halo merger wherein both halos have been seeded will also result in a prompt BH merger, which represents a highly optimistic merger scenario. The effects of a more realistic inspiral via the effects of dynamical friction are investigated in a future work by [Bhowmick et al. \(in prep\)](#).

For further details regarding the models used here, please see [Bhowmick et al. \(2024c\)](#) and references therein.

2.2. Black hole seeding prescriptions

The key feature distinguishing BRAHMA from TNG is the prescriptions for seeding BHs within subhalos. In this study, we use four simulations that include increasingly restrictive seed models by stacking the seeding requirements described below. In all four boxes, BHs are seeded with an initial seed mass of $M_{\text{seed}} = 1.5 \times 10^5 M_{\odot}$. The criteria imposed are motivated based on conditions expected for direct collapse black hole (DCBH) formation and are as follows:

1. *Halo mass criterion:* BHs can only be seeded within subhalos that are resolved. The requirement for BRAHMA subhalos to be resolved is 32 DM particles, which corresponds to a halo mass of $4.8 \times 10^7 h^{-1} M_{\odot}$.
2. *Dense and metal-poor gas mass criterion:* Seeds are placed in halos that exceed a minimum amount of gas mass ($5 \times M_{\text{seed}}$) in local pockets of dense ($\rho > 0.13 \text{ cm}^{-3}$) and metal-poor ($Z < 10^{-4} Z_{\odot}$) gas.
3. *Lyman-Werner flux criterion:* The dense and metal-poor gas is additionally required to be exposed to an incident Lyman-Werner (LW) flux greater than $J_{\text{crit}} = 10 J_{21}$. The critical LW flux (J_{crit}) used here is significantly lower than values suggested by small scale simulations and one-zone chemistry models (Shang et al. 2010; Sugimura et al. 2014), who report a necessary intensity of $\geq 1000 J_{21}$. But as shown in Bhowmick et al. (2024c), to produce overmassive BHs consistent with JWST, we need more abundant heavy seed formation. Therefore, we used a low value of J_{21} that has been shown to be feasible if gas is dynamically heated during major mergers (Regan et al. 2020b,a; Wise et al. 2019).
4. *Gas spin criterion:* With the addition of this criteria, halos must have a sufficiently low spin parameter, defined by

$$\lambda = \frac{|\vec{J}_{\text{spin}}|}{\sqrt{2} M_{\text{gas}} R_{\text{vir}} V_{\text{vir}}} < \lambda_{\text{max}}, \quad (1)$$

where \vec{J}_{spin} is the spin of the gas in dimensionless units, M_{gas} , R_{vir} , and V_{vir} are the gas mass, virial radius, and circular velocity, and λ_{max} is at the onset of the Toomre instability respectively (Toomre 1964). This stability criterion was based on the analysis done by Lodato & Natarajan (2006), who studied the stability of pre-galactic disks and the conditions necessary for the disk’s collapse into a DCBH.

5. *Halo environment criterion:* This criterion ensures that seeds are placed in halos that have a “rich” environment. This means that the halo must have at least one halo of comparable or greater mass within five times its virial radius. This criterion is designed to seed exclusively in environments where halos are more likely to undergo major mergers that could dynamically heat gas, thereby justifying the feasibility of our adopted low J_{crit} value.

For more details on the implementation of the Lyman-Werner flux/gas spin and halo environment criteria, please see Bhowmick et al. (2022a) and Bhowmick et al. (2024a), respectively. While all four simulations employ the halo mass criterion, the first simulation, which we refer to as BI, only additionally employs the dense and metal-poor criterion. The second simulation, BII, includes both the dense and metal-poor criteria as well as the Lyman-Werner flux criteria. The third simulation, BIII, includes both of the previous criteria, as well as the low spin criterion. Finally, the fourth simulation, which adds the rich environment criterion, we refer to as BIV. Note that in Bhowmick et al. (2024c) these same simulations were referred to as SM5, SM5_LW10, SM5_LW10_spin, and SM5_LW10_spin_rich respectively.

In order to understand the effects that these above “gas based” seeding criterion have on the scaling relations, we compare our simulation results to the scaling relations for the TNG (Nelson et al. 2018; Pillepich et al. 2018b; Naiman et al. 2018; Marinacci et al. 2018; Springel et al. 2018) simulation that uses the standard “halo mass threshold-based” seeding. BHs are seeded with mass $8 \times 10^5 h^{-1} M_{\odot}$ in TNG in halos with masses greater than $5 \times 10^{10} h^{-1} M_{\odot}$ (Weinberger et al. 2017; Vogelsberger et al. 2013). This condition is significantly more restrictive than BRAHMA’s minimum halo mass requirement of $4.8 \times 10^7 h^{-1} M_{\odot}$.

To demonstrate the impact of the various seeding prescriptions, we show the redshift evolution of the comoving BH number density for our four seeding models in Fig. 1. As one might expect, imposing increasingly restrictive seeding criteria reduces the number density of BHs in each subsequent simulation at all redshifts. Increasingly restrictive seeding criteria also delay the onset of seeding to somewhat later redshifts. All four curves show a characteristic maximum number density at redshifts of approximately $z \sim 6 - 10$, which is due to a balance between BH seeding and BH mergers, as well as metal enrichment at low- z . At early times, the BH seeding rate is much greater than the merger rate of seeded halos (since very few halos have yet to be seeded), causing the number density to increase. As halos continue to be seeded in increasing numbers until $z \lesssim 10$ and then

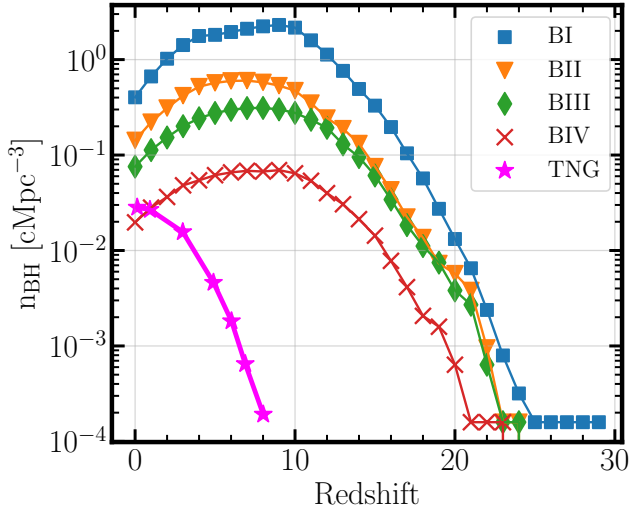


Figure 1. BH number density in comoving Mpc^{-3} for each of the four BRAHMA simulations as a function of redshift. With each incrementally more restrictive seed model, the number density of BHs decreases at all redshifts, and halos start to be seeded at later times. The onset of seeding and number density of BHs in TNG is greatly reduced due to its extremely restrictive halo mass requirement. Since the more restrictive seed models have much fewer BH seeds, their growth via mergers is significantly reduced.

merge, the reduction in the BH number densities due to mergers greatly increases, resulting in a maximum number density followed by a gradual decline for all four simulations. For the TNG simulation, plotted for comparison, the onset of seeding and peak number density is greatly delayed due to the extremely restrictive halo mass criterion. Because of the simple seeding criterion, the number of halos being seeded in TNG still increases at later times ($z < 10$).

2.3. The σ calculation

We calculate the velocity dispersion as the mass-weighted velocity dispersion of all of the stars in the bulge of the galaxy. To identify the stars that belong to the bulge, we perform a kinematic decomposition as done in Huang et al. (2018) and Abadi et al. (2003). A metric $\kappa = j/j_{\text{max}}(e)$ is calculated for every star in the galaxy, where j is the star’s specific angular momentum, and $j_{\text{max}}(e)$ is the maximum specific angular momentum for a star with specific binding energy e . The specific binding energy of a star particle is defined as the energy required to make the star an unbound particle, and was calculated as the sum of the specific kinetic and potential energies. Stars with $\kappa > 0.5$ are considered to be a part of the disk of the galaxy, in following with Du et al. (2019, 2020). Stars with $\kappa < 0.5$ are considered a part of the bulge, and used in our stellar mass and

σ calculations. To allow for a proper comparison between our σ calculations and observed line-of-sight σ ’s, in all of our plots we show a one dimensional σ calculated as $\sigma_{1D} = \frac{\sigma_{3D}}{\sqrt{3}}$. Here, $\sigma_{3D} = \sqrt{\sigma_x^2 + \sigma_y^2 + \sigma_z^2}$, where $\sigma_x, \sigma_y, \sigma_z$ are the stellar velocity dispersions in the $x, y,$ and z directions respectively.

In keeping with Huang et al. (2018), we only retain subhalos with greater than 1000 stars in our sample for TNG, as the decomposition may not produce well-defined bulge and disk components below this number. However, we apply the decomposition indiscriminately to all subhalos in the BRAHMA simulations, as imposing a 1000 star criterion would eliminate most, if not all, subhalos in our simulations at high redshift. We thus apply the decomposition to all BRAHMA subhalos for each redshift, regardless of the number of stars in each subhalo. The decomposition is performed based on the energetics of individual star particles relative to their gravitational potential environment. Each star particle is classified as being on a ‘bulge-like’ or ‘disk-like’ orbit to recover the spheroidal component of lower-mass galaxies. We note that while this method is imperfect, it yields reasonable cuts for the bulge component of most galaxies in our sample. It is also worth noting that while we perform this decomposition to have bulge stellar masses and velocity dispersions to allow for comparison to the observed scaling relations, photometrically derived bulge-disk decompositions may differ from kinematically derived decompositions, especially for lower stellar mass systems (see Fig. 7 of Bottrell et al. 2017).

The scripts used to perform this decomposition and the rest of the analysis in this work are publicly available at https://github.com/khojonat/Brahma_Analysis.

3. RESULTS

3.1. Impact of seeding on the $M_{\bullet} - \sigma$ relation

We begin by showing in Fig. 2 2D histograms of the $M_{\bullet} - \sigma$ relation for the most lenient (BI) and most strict (BIV) seeding models at redshifts $z = 5, 0$. The blue and red lines trace the median BH mass and interquartile range for different σ bins. In all of our figures, we also include the local scaling relations for $M_{\bullet} - \sigma$ and $M_{\bullet} - M_{\star}$ as found by Kormendy & Ho 2013 (hereafter KH13), the high- z $M_{\bullet} - M_{\star}$ relation found by Pacucci et al. (2023) (hereafter, P23), and a population of recently detected high-redshift AGN as reported by Maiolino et al. (2024b) and Juodžbalis et al. (2025). We will first discuss the trends exhibited by the different simulations in this section, followed by how they compare against observations in Section 4.1.

Fig. 2 shows the range of velocity dispersions that our boxes can probe at different redshifts, which is nat-

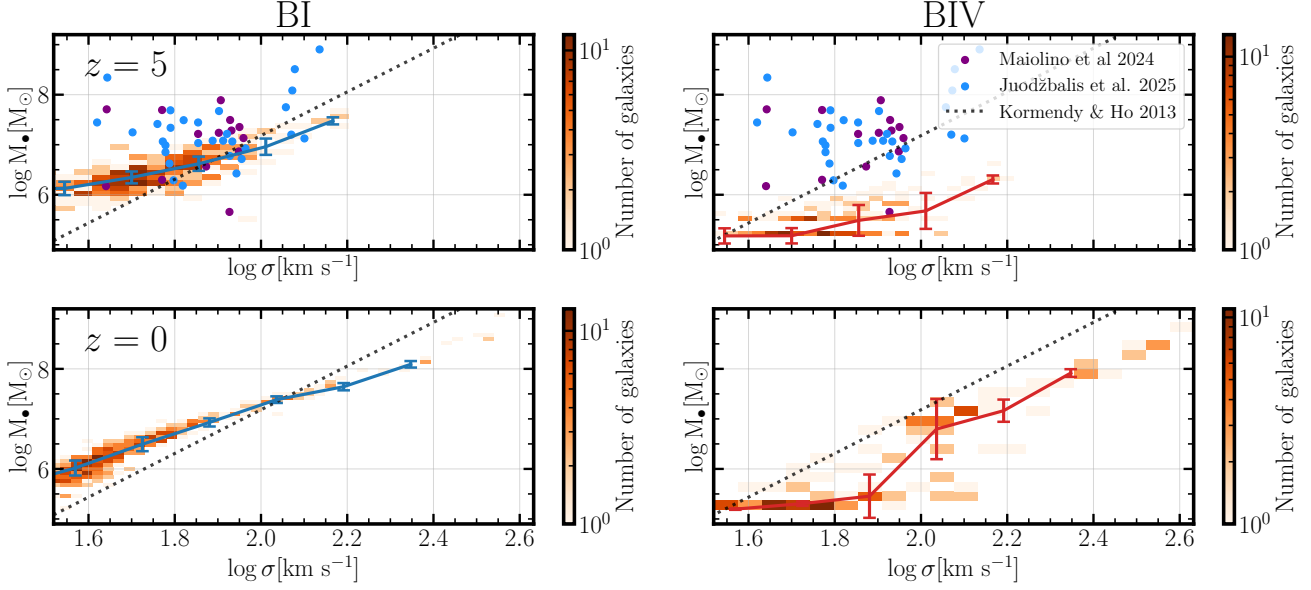


Figure 2. Histograms of the full scatter of BHs for the most lenient and most restrictive seed models on the $M_{\bullet} - \sigma$ relation. Plotted in blue and red is the median trend of the data, with error bars representing the interquartile range in BH mass. The dotted line shows the observed $M_{\bullet} - \sigma$ by KH13. While the relation retains a tight correlation for the most lenient model across redshift, the scatter drastically increases with decreasing redshift for the most strict model at intermediate values of σ .

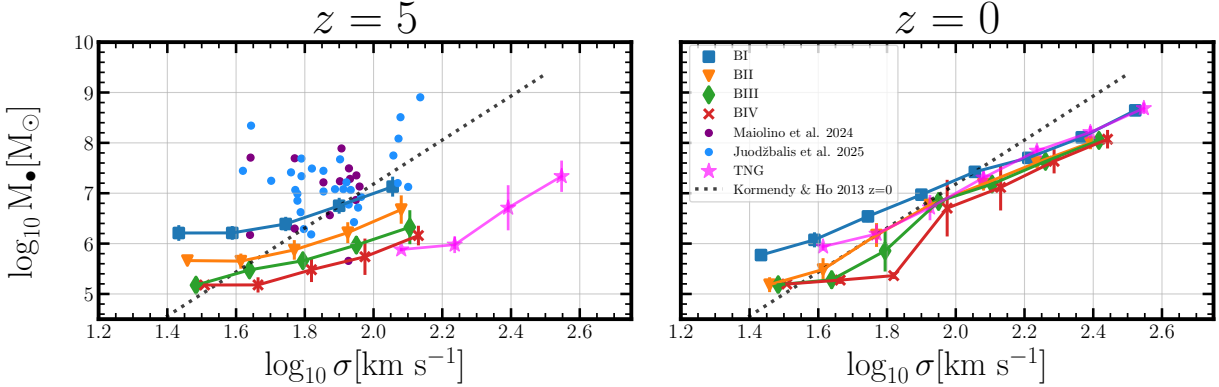


Figure 3. Comparison of the BRAHMA and TNG simulations' $M_{\bullet} - \sigma$ relations at $z = 5, 0$. The local relation found by KH13 is plotted in both panels for reference, and high- z AGN candidates found by Maiolino et al. (2024b) and Juodžbalis et al. (2025) are shown in purple and blue in the $z = 5$ panel. With the exception of our most lenient seed model, the simulations all begin under-massive to the local relation at high- z and converge to this relation by $z = 0$. The different BRAHMA seed models are clearly differentiable for all σ 's at $z = 5$ via their different normalizations, and are still differentiable for $10^{1.7} \text{ km s}^{-1} \lesssim \sigma \lesssim 10^{1.9} \text{ km s}^{-1}$ at $z = 0$.

urally limited by our volume and resolution. At $z = 5$, our BRAHMA boxes are able to probe σ values between $\sim 10^{1.5} - 10^{2.2} \text{ km s}^{-1}$, whereas at $z = 0$ they probe $\sim 10^{1.5} - 10^{2.6} \text{ km s}^{-1}$.

Most interestingly, we can clearly see that the BH masses are substantially different between the seed models, thereby impacting the median as well as the scatter of the $M_{\bullet} - \sigma$ relation. At $z = 5$, we find that the most lenient BI model produces a substantially higher $M_{\bullet} - \sigma$ normalization (higher BH mass at fixed σ) com-

pared to the most restrictive BIV model. In the left panel of Figure 3, we can see this trend more readily as the median trends for all four seed models are plotted together. This is because in the more lenient seed models, there is stronger merger-driven BH growth due to the higher number of seeds. To that end, Bhowmick et al. (2024c) and Bhowmick et al. (2025) showed that at these high redshifts, the BH mass assembly is dominated by mergers in these simulations. In fact, TNG, which has the most restrictive seed model, produces a

lower $M_\bullet - \sigma$ than all the BRAHMA boxes (albeit TNG probes much higher σ values due to lower resolution and a larger volume). This is simply because too few seeds are produced in TNG to fuel enough merger-driven growth.

By $z = 0$, the $M_\bullet - \sigma$ relations show substantially reduced seed model variations, particularly for $\sigma \gtrsim 80 \text{ km s}^{-1}$ (bottom panels of Figure 2 and right panel of Figure 3). These high σ values correspond to more massive galaxies, where Bhowmick et al. (2025) found that BH mass assembly is dominated by gas accretion, in line with the expectations from the Soltan Argument (Soltan 1982). However, seed model variations are much more substantial at low σ values between 50 to 80 km s^{-1} . This is because for these low σ values corresponding to lower mass ($\lesssim 10^9 M_\odot$) galaxies, Bhowmick et al. (2025) showed that BH growth continues to be dominated by mergers all the way down to $z = 0$.

Overall, we find that the median $M_\bullet - \sigma$ relations show the strongest seed model variations at $z = 5$ across all σ values probed by our simulations, and at $z = 0$ for low σ values ($\sim 50\text{--}80 \text{ km s}^{-1}$). These variations primarily arise from differences in the ability to fuel merger-driven BH growth under the various seeding models.

3.2. Redshift evolution of the median $M_\bullet - \sigma$ relation: Relationship to $M_\bullet - M_*$

In this section, we delve deeper into the redshift evolution of the median $M_\bullet - \sigma$ relation for the different seed models and how it connects to the $M_\bullet - M_*$ and $M_* - \sigma$ relations. Fig. 4 simultaneously shows the three scaling relations ($M_\bullet - \sigma$, $M_\bullet - M_*$, and $M_* - \sigma$) for each of our BRAHMA boxes, as well as for TNG. Notably, for the most lenient seed model, the median $M_\bullet - \sigma$ relation (1st row, left panel) is largely insensitive to redshift. For the more restrictive seed models, the $M_\bullet - \sigma$ evolution follows a “bottom-up” trend at high σ ($\gtrsim 100 \text{ km s}^{-1}$) i.e. BH masses are lower at earlier times. The evolution is much weaker at the low σ end. Continuing this trend, the TNG seed model, being even more restrictive than BIV, produces a bottom-up $M_\bullet - \sigma$ evolution which is even more pronounced than the BRAHMA boxes.

While the $M_\bullet - \sigma$ evolution proceeds in a bottom-up fashion for most of our models, the $M_\bullet - M_*$ relation (middle column of Fig. 4) exhibits a ‘top-down’ evolution across all BRAHMA boxes—that is, BH masses are higher at earlier times at fixed stellar mass. This evolution is seen primarily for galaxies in the $\sim 10^7\text{--}10^9 M_\odot$ range, as more massive systems are not accessible in our BRAHMA volumes at higher redshifts. As shown in Bhowmick et al. (2025), BH growth in these relatively low-mass galaxies is dominated by mergers down to

$z \sim 0$. In such systems, the top-down evolution of the $M_\bullet - M_*$ relation arises naturally from this merger-driven BH growth: while BHs grow mainly via mergers, stellar mass increases more rapidly due to a combination of in-situ star formation and mergers. Notably, in contrast to the top-down $M_\bullet - M_*$ evolution seen in BRAHMA, the TNG relation (Fig. 4, bottom row) shows a bottom-up evolution. This is due to (1) a significantly lower BH seed abundance in low-mass galaxies, which suppresses merger-driven BH growth at $M_* \lesssim 10^9 M_\odot$, and (2) the fact that we show only galaxies with $M_* \gtrsim 10^9 M_\odot$ (due to the 1000 star-particle cut in the kinematic decomposition), where BH growth is dominated by accretion, which outpaces stellar mass growth from $z \sim 5$ to 0.

To explain why for the BRAHMA boxes, the $M_\bullet - \sigma$ evolution does not simply follow the top-down trend of the $M_\bullet - M_*$ evolution, we show the $M_* - \sigma$ relation in the right column of Figure 4. The seed models have a negligible effect on the $M_* - \sigma$ relation, likely because BH accretion (and therefore, AGN feedback) is too weak to have any significant influence on stellar mass assembly, especially in lower mass galaxies $M_* \lesssim 10^9 M_\odot$. Importantly, regardless of the seed model, galaxies at fixed stellar mass exhibit higher velocity dispersions at higher redshifts. The key driver of this trend is that, at fixed M_* , galaxies are more compact at higher redshifts (see Appendix A for more details). This evolution of $M_* - \sigma$ competes with the top-down $M_\bullet - M_*$ evolution, and as a result, prevents a top-down evolution in $M_\bullet - \sigma$.

However, since there are no seed model variations in $M_* - \sigma$, its evolution alone does not explain the seed model variations within the $M_\bullet - \sigma$ evolution. More specifically, it is not yet clear why we see negligible $M_\bullet - \sigma$ evolution for the most lenient seed model, and a bottom-up evolution (at the high σ end) for more restrictive seed models. To better understand the connection between the evolution of the $M_\bullet - \sigma$ relation and that of the $M_\bullet - M_*$ and $M_* - \sigma$ relations, we expand the time derivative of the median BH mass, \bar{M}_\bullet (in logarithmic units), at fixed σ as

$$\left. \frac{d\bar{M}_\bullet}{dt} \right|_\sigma = \left. \frac{\partial \bar{M}_\bullet}{\partial M_*} \right|_{t,\sigma} \cdot \left. \frac{dM_*}{dt} \right|_\sigma + \left. \frac{\partial \bar{M}_\bullet}{\partial t} \right|_{M_*,\sigma} \quad (2)$$

Here, \bar{M}_\bullet at fixed σ is treated as a function of both stellar mass M_* and cosmic time t . In taking the total derivative $d\bar{M}_\bullet/dt$, we are tracking the evolution of \bar{M}_\bullet across BH subsamples at fixed σ , but not at fixed M_* . Figure 5 shows this evolution of \bar{M}_\bullet across time for different σ bins. While this figure does not present fundamentally new information beyond what was shown in Figure 4, it enables a closer examination of how the $M_\bullet - \sigma$ relation evolves as a function of σ and seed model.

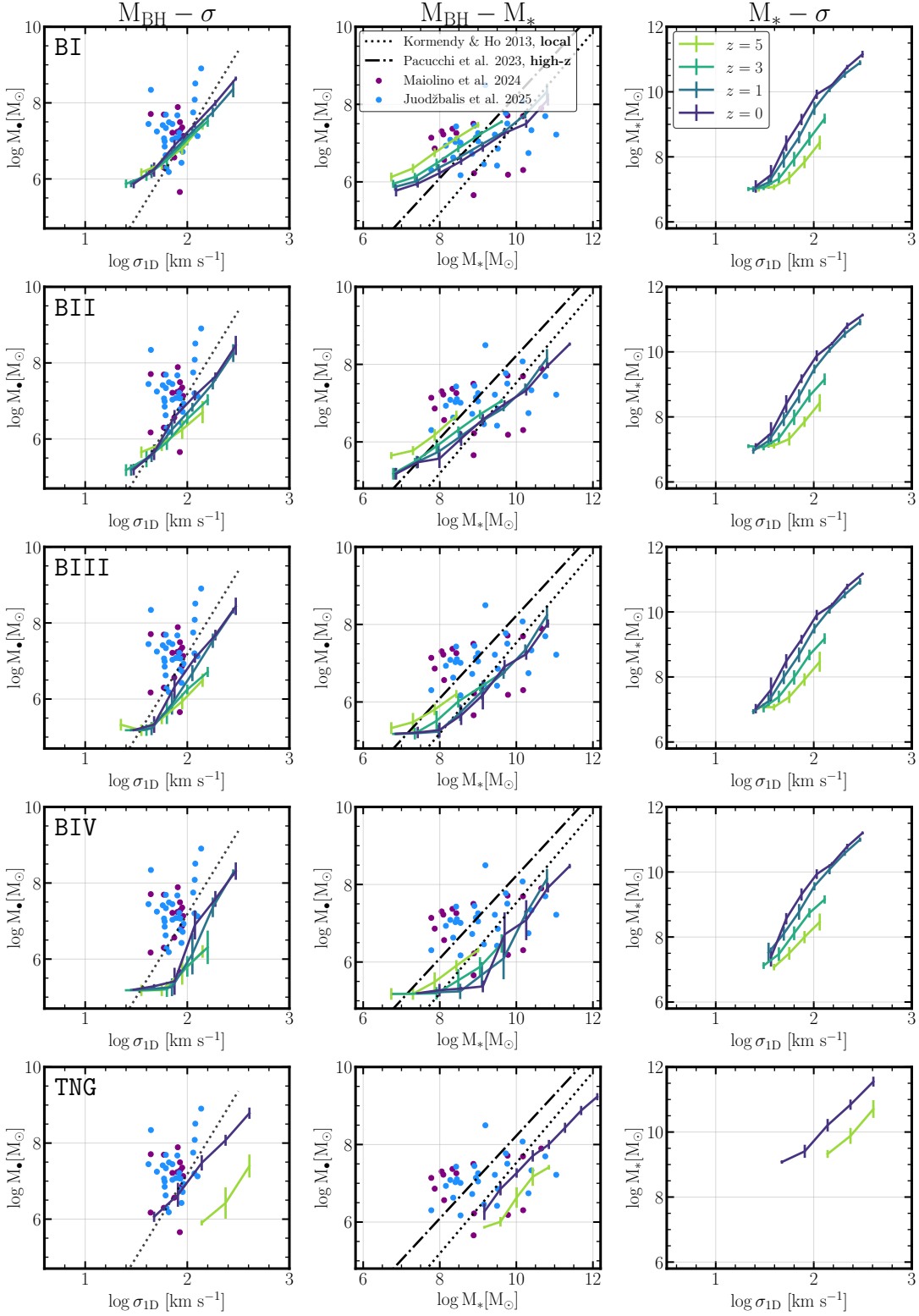


Figure 4. The $M_* - \sigma$, $M_* - M_*$, and $M_* - \sigma$ relations for the four BRAHMA boxes and TNG. Each plot shows the relation for redshifts $z = 5, 3, 1, 0$ to provide a sense of their redshift evolution. The $M_* - \sigma$ and $M_* - M_*$ columns show the local relations as reported by KH13, and the $M_* - M_*$ plots additionally show the high- z inferred relation found by P23. These columns also show high- z AGN as reported by Maiolino et al. (2024b) and Juodžbalis et al. (2025).

In particular, we can clearly see that the evolution of \bar{M}_\bullet is increasingly steep for $\sigma = 100 \text{ km s}^{-1}$ as the seed model becomes more restrictive. Notably, for the more restrictive seed models, almost all of this evolution occurs after $z \sim 2$.

To understand how these trends relate to the $M_\bullet - M_*$ and $M_* - \sigma$ evolution, we now consider the three components on the right-hand side (RHS) of Eq. 2:

- **Component 1** is $\left. \frac{d\bar{M}_\bullet}{dt} \right|_\sigma$, which captures the evolution of stellar mass in galaxies within fixed- σ subsamples. This essentially corresponds to the evolution of the $M_* - \sigma$ relation.
- **Component 2** is $\left. \frac{\partial \bar{M}_\bullet}{\partial M_*} \right|_{t,\sigma}$, which measures the dependence of BH mass on stellar mass at fixed time and σ . As explained in Appendix B, this term can be reasonably approximated by the slope of the $M_\bullet - M_*$ relation.
- **Component 3** is $\left. \frac{\partial \bar{M}_\bullet}{\partial t} \right|_{M_*,\sigma}$, which represents the explicit time evolution of \bar{M}_\bullet at fixed M_* and σ .

In Figure 7, we study the interplay among the three components described above in determining the distinct evolution seen in the $M_\bullet - \sigma$ relation for different seed models. Note that we present the derivatives with respect to decreasing redshift (i.e., increasing cosmic time), as required by Eq. 2.

Component 1 (Figure 7a) shows negligible dependence on seeding, as also seen in column 3 of Figure 4. Therefore, differences between seed models in the $M_\bullet - \sigma$ evolution must originate from Components 2 and 3 (Figures 7b and 7c, respectively). Since component 1 is always positive, the relative signs of components 2 and 3 determine whether they cancel or reinforce each other, depending on the seed model. For both components, the dependence on redshift becomes stronger with more restrictive seeding. This also leads to significant differences in the interplay between components 2 and 3 across redshift for the different seed models. For the most lenient seed model, the combination of components 1 and 2 nearly cancels with component 3 at all redshifts, as components 1 and 2 remain positive and component 3 remains negative throughout (compare the blue line in Figure 7b with the leftmost panel in Figure 7c), explaining why this seed model produces the weakest $M_\bullet - \sigma$ evolution. In contrast, for the most restrictive seed model, component 2 remains positive and increases toward lower redshift (red line in Figure 7b), while component 3 rises steeply around $z \sim 2$, transitioning from negative to positive for $\sigma = 10^{1.75}$ and $\sigma = 10^2 \text{ km s}^{-1}$ (middle and right panels of Figure 7c). As a result, the two components tend to cancel at $z \gtrsim 2$

but strongly reinforce each other at $z \lesssim 2$. This naturally explains the behavior for $\sigma = 100 \text{ km s}^{-1}$ in Figure 5 (rightmost panel), where the most restrictive seed model shows weak evolution in $M_\bullet - \sigma$ up to $z \sim 2$, followed by a steep increase between $z \sim 2$ and $z = 0$. All this also explains the evolution seen in the intermediate BII and BIII seed models, which are qualitatively similar to BIV but exhibit a less steep rise at $z \lesssim 2$. In Figure 9, we explicitly confirm that these trends fully account for the evolution of M_\bullet at fixed σ .

3.2.1. Physical drivers of the seed model variations in the $M_\bullet - \sigma$ evolution

Now that we have isolated the contributions of Components 2 and 3 to the evolution of the median $M_\bullet - \sigma$ relation, we can investigate the implications of this analysis on the physics of BH growth. We begin with Component 2, which describes the evolution of the $M_\bullet - M_*$ relation. Figure 7b shows how the slope of the $M_\bullet - M_*$ relation remains roughly constant with time for the lenient seed models and strongly steepens with time for the more restrictive seed models. As a result, the $z \lesssim 2$ slopes are higher for the restrictive seed models. All these trends are a natural consequence of the merger-dominated BH growth in low-mass ($\lesssim 10^9 M_\odot$) galaxies. In particular, as the seed models become more restrictive, BH-BH mergers are suppressed, and galaxy growth outpaces BH growth disproportionately more strongly in low-mass galaxies, compared to more massive galaxies where BHs can grow via accretion. We can readily see how these processes steepen the $M_\bullet - M_*$ slope at $z \lesssim 2$ in the middle panels of Figure 4.

We now discuss Component 3, which tracks how BH masses evolve with redshift at fixed M_* and σ . The fact that this component is predominantly negative at high redshift is a direct consequence of merger-driven BH growth, where galaxy growth naturally outpaces BH growth. In particular, because both M_* and σ grow more rapidly than M_\bullet , the latter appears to decrease with time when viewed at a fixed bin on the $M_* - \sigma$ plane. However, at $z \lesssim 2$, this component starts to increase and becomes positive by $z \sim 0$ for high σ ($\sigma \sim 100 \text{ km s}^{-1}$). This is because in these high $\sigma \sim 100 \text{ km s}^{-1}$ and massive $\gtrsim 10^9 M_\odot$ galaxies at $z \lesssim 2$, accretion-driven BH growth accelerates and outpaces the growth in M_* . Therefore, for the most restrictive BIV seed model, with the smallest amount of merger-driven growth, we see the strongest spike in component 3 at $z \lesssim 2$ for $\sigma = 100 \text{ km s}^{-1}$ in the rightmost panel of Fig. 7c.

Overall, we find that the evolution of the $M_\bullet - \sigma$ relation can be summarized as follows: The $M_\bullet - \sigma$ relation undergoes negligible evolution from $z \sim 5 - 0$

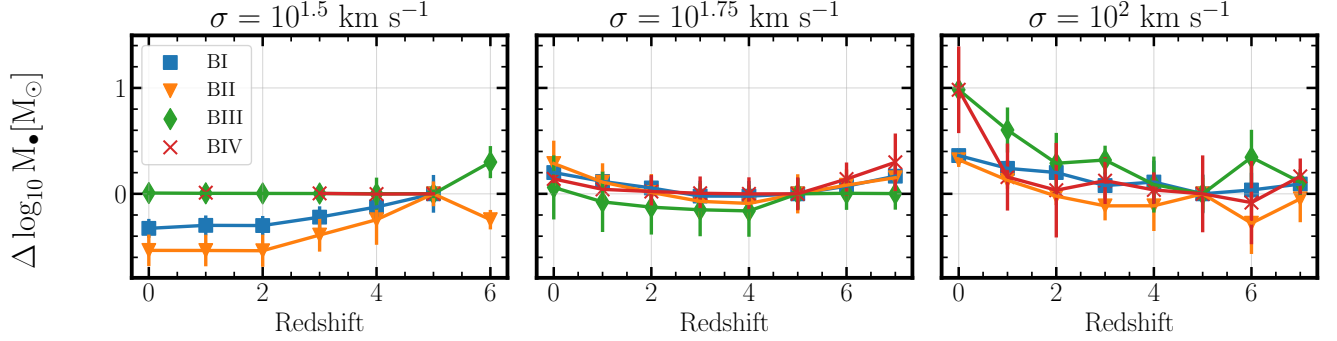


Figure 5. Redshift evolution of the median BH mass for the four BRAHMA simulations at fixed σ values. All lines have been normalized to the median BH mass at $z = 5$ to emphasize the different evolutions. Errorbars represent 95% confidence intervals about the median mass calculated via bootstrapping of the data. We clearly see here a negative redshift evolution for the more lenient seed models at $\sigma = 10^{1.5} \text{ km s}^{-1}$, very minimal redshift evolution for all seed models at $\sigma = 10^{1.75} \text{ km s}^{-1}$, and a stronger positive redshift evolution for more restrictive seed models at $\sigma = 10^2 \text{ km s}^{-1}$. At $\sigma = 10^2 \text{ km s}^{-1}$, for the more restrictive seed models, the increase in median BH mass occurs almost entirely at $z < 2$.

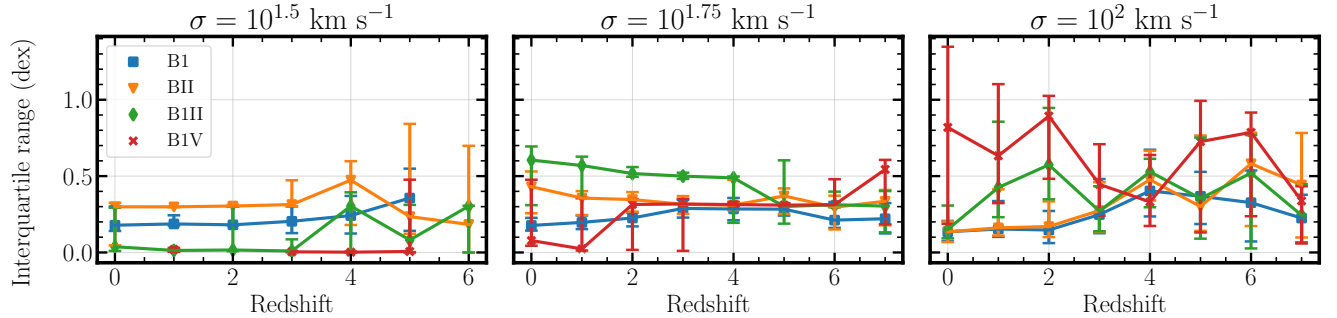


Figure 6. Redshift evolution in the scatter (shown using the interquartile range (IQR)) of the $M_{\bullet} - \sigma$ relation for subhalos of fixed σ . Errorbars again represent 95% confidence intervals calculated via bootstrapping. With increasingly more restrictive seed models, the scatter and the variation in the scatter across all redshifts tends to increase for $\sigma = 10^2 \text{ km s}^{-1}$, while the scatter remains very small at $\sigma = 10^{1.5} \text{ km s}^{-1}$ for the more restrictive seed models.

for the most lenient BI seed model. For the most restrictive seed BIV model, there is a bottom-up evolution to $z \sim 0$, with the majority of the evolution occurring for massive galaxies ($\gtrsim 10^9 M_{\odot}$) at high sigma end ($\sigma > 100 \text{ km s}^{-1}$) at $z \lesssim 2$. These evolutionary trends are a consequence of the merger-dominated BH growth in low mass ($\lesssim 10^9 M_{\odot}$) galaxies and accretion dominated growth in high mass ($\gtrsim 10^9 M_{\odot}$) galaxies, as identified in Bhowmick et al. (2025).

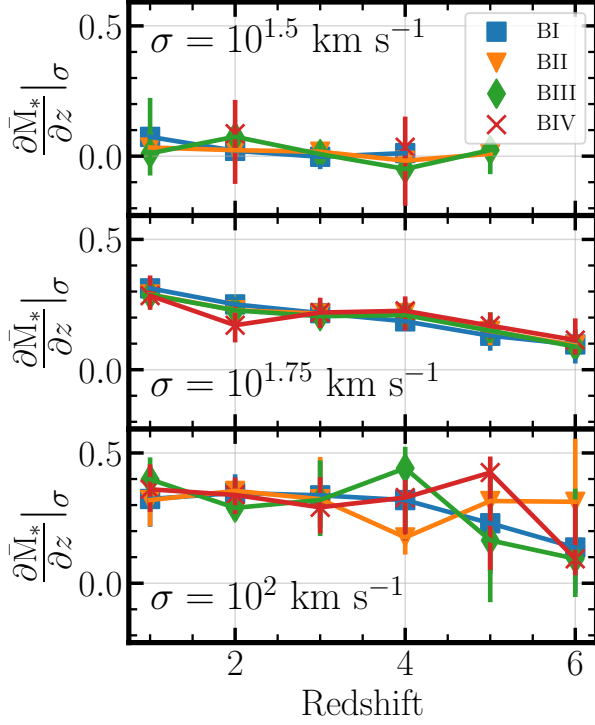
3.3. The redshift evolution in the scatter of the $M_{\bullet} - \sigma$ relation

Having studied the median $M_{\bullet} - \sigma$ relation, we now study the redshift evolution of the scatter for different BH seed models. We quantify this scatter by the Interquartile Range (IQR). Its evolution is plotted at fixed σ in Fig. 6. Immediately, one can tell that the most lenient seed model has very little evolution in the scatter for all values of σ . However, as seed models

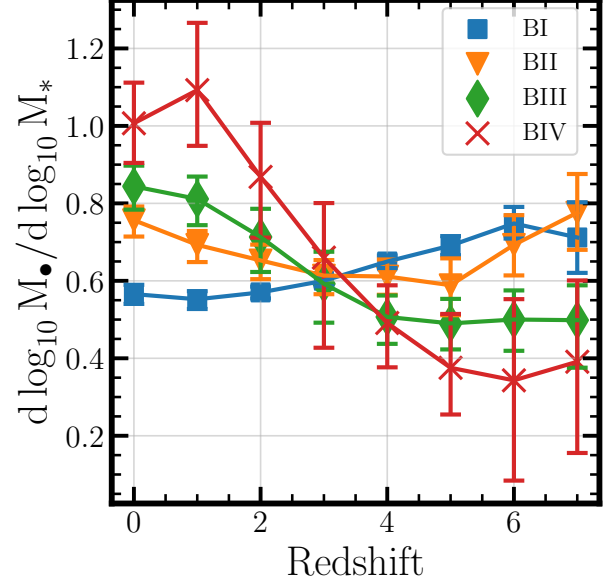
become more restrictive, the overall scatter tends to increase for $\sigma = 10^2 \text{ km s}^{-1}$, while staying small for $\sigma = 10^{1.5}, 10^{1.75} \text{ km s}^{-1}$.

For low $\sigma = 10^{1.5} \text{ km s}^{-1}$, the scatter becomes small for the two most restrictive seed models because the population of subhalos with this dispersion consist entirely of BHs that have grown very little past their initial seed mass. The galaxies that do see their BHs grow significantly have also all grown significantly in σ . Therefore, only the ungrown BHs are left in subhalos with $\sigma \sim 10^{1.5} \text{ km s}^{-1}$.

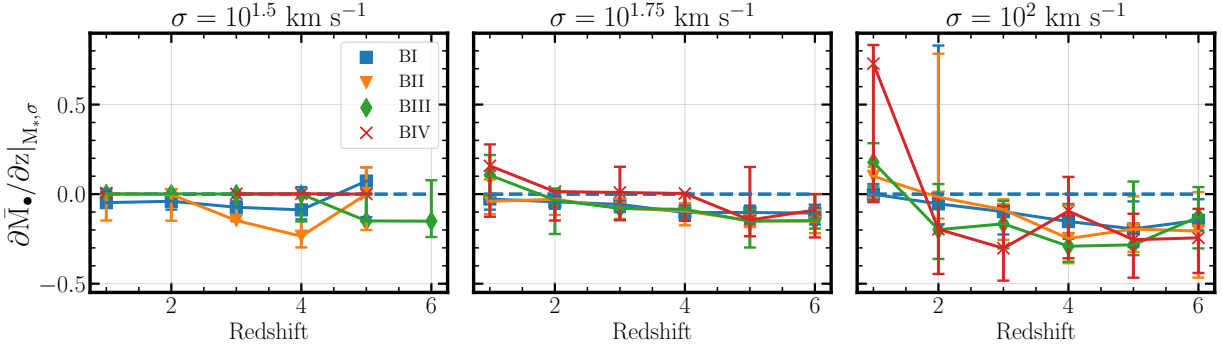
At high $\sigma = 100 \text{ km s}^{-1}$, the larger scatter in the more restrictive seed models is also due to the stronger presence of ungrown BH seeds within more massive galaxies. More specifically, the increase in scatter is due to presence of *both* grown as well as ungrown seeds in the more massive galaxies, which “puffs up” the $M_{\bullet} - \sigma$ relation as shown in Figure 2. In contrast, for the more lenient seed models, almost all the seeds are able to readily grow



(a) The change in stellar mass with decreasing redshift at fixed σ values. The trends seen for each σ value are very similar between BRAHMA boxes. Generally, M_* increases with decreasing redshift at fixed σ , with lower σ values showing weaker redshift evolution.



(b) Redshift evolution of the slope of the $M_{\bullet} - M_*$ relation for each of the four BRAHMA simulations. At $z \sim 3$, there is a strong inversion in slope ordering: initially, more lenient seed models had larger slopes, whereas at later times, more restrictive models show much steeper slopes. This evolution is a key factor behind the changing $M_{\bullet} - \sigma$ relation.



(c) Explicit redshift dependence of median BH mass at constant σ and M_* . Highlighted in a blue dashed line is $\partial M_{\bullet} / \partial z = 0$. For almost all redshifts for all seed models, the change in BH mass with redshift is negative. The sharp increase in $\partial M_{\bullet} / \partial z$ at late times for the more restrictive models constitutes the other major contribution to a redshift-evolving $M_{\bullet} - \sigma$ relation.

Figure 7. The evolution of the different components that determine the redshift evolution of the $M_{\bullet} - \sigma$ relation, as identified in Equation 2. Errorbars in each panel represent 95% confidence intervals about the derivative being shown, obtained via bootstrapping of the data.

and settle close to the local $M_{\bullet} - \sigma$ relation, leading to smaller scatter.

Unfortunately, our small volume significantly limits our ability to fully probe the $M_{\bullet} - \sigma$ relation. To that end, we show bootstrapped errors for the IQR as errorbars in Fig. 6. Here, we clearly see these errorbars grow larger for more restrictive seed models, suggesting that there is some stochasticity in our current IQR values due to poor statistics. With a larger volume, we would expect this stochastic variation to be diminished, but the seed model variations in the scatter discussed in the previous paragraphs should remain.

4. DISCUSSION

4.1. Implications from observational measurements of $M_{\bullet} - \sigma$

Having understood the evolution of the $M_{\bullet} - \sigma$ relation and its drivers, we now compare against currently available observations. At $z \sim 0$, the seed model variations are most pronounced for our lower-mass BHs ($M_{\bullet} \lesssim 10^7 M_{\odot}$) in galaxies with velocity dispersions $\sigma \sim 50\text{--}80 \text{ km s}^{-1}$. It is therefore useful to compare with observed local relations such as KH13, keeping in mind that these are based almost entirely on more massive BHs with $M_{\bullet} \gtrsim 10^7 M_{\odot}$. The intermediary BII and BIV seed models show reasonably good agreement with the “extrapolated” KH13 relation (Fig. 3, right panel). The most lenient BI model yields a shallower slope and higher normalization than KH13 at $\sigma \sim 50\text{--}80 \text{ km s}^{-1}$, while the most restrictive BIV seed model produces lower normalizations. Similar conclusions arise when comparing the $M_{\bullet} - M_{*}$ relations with observations (see middle panels of Fig. 4). For our massive BHs ($\gtrsim 10^8 M_{\odot}$) at $z = 0$, the median $M_{\bullet} - \sigma$ relation shows a lower normalization compared to KH13. This is also the case for the TNG simulations. Since seed model variations are minimal for massive BHs at $z \sim 0$, these discrepancies likely have stronger implications on the BH accretion and feedback models rather than the seed models, which is beyond the scope of this work.

At higher redshifts, we present the $z \sim 4\text{--}7$ JWST BLAGN on the $M_{\bullet} - \sigma$ plane, as measured by Maiolino et al. (2024b) and Juodžbalis et al. (2025). Remarkably, these studies find that the high- z JWST AGN lie close to the local $M_{\bullet} - \sigma$ relation, yet appear significantly overmassive on the $M_{\bullet} - M_{*}$ plane. This observation aligns strikingly well with our most lenient BI seed model, which produces similarly overmassive $z \sim 5$ BHs consistent with JWST data on the $M_{\bullet} - M_{*}$ relation, while simultaneously exhibiting negligible evolution in the $M_{\bullet} - \sigma$ relation. The BI seed model’s $M_{\bullet} - \sigma$ relation is also broadly consistent with the high- z JWST AGN.

Conversely, the more restrictive seed models, which predict bottom-up growth, systematically under-predict the $M_{\bullet} - \sigma$ relation compared to the JWST AGN.

Of course, uncertainties remain in the measurements of black hole mass, stellar mass, and stellar velocity dispersion for high- z JWST AGN and their host galaxies. These include the possibility of BH mass overestimation (Rusakov et al. 2025; Naidu et al. 2025), as well as potential underestimation of stellar masses due to uncertainties in modeling the AGN contribution (Ramos Padilla et al. 2020). Additionally, while stellar velocity dispersions are not directly measured at these redshifts, they are inferred from gas velocity dispersion measurements using a correction factor of 1.3 (see Section 5.1 of Juodžbalis et al. 2025). Despite these uncertainties, our main conclusions regarding the impact of seeding on the $M_{\bullet} - \sigma$ relation and its evolution remain robust. Should these observational measurements stand the test of time, our most lenient seed model offers a natural explanation for the existence of high- z BHs that appear overmassive relative to the local $M_{\bullet} - M_{*}$ relation, while still being entirely consistent with the local $M_{\bullet} - \sigma$ relation.

Another way to express the above results is to note that assembling the local $M_{\bullet} - \sigma$ relation as early as $z \gtrsim 5$ —as suggested by JWST measurements—requires the abundant formation of heavy $\sim 10^5 M_{\odot}$ seeds. Forming such seeds is challenging under canonical direct collapse black hole (DCBH) formation channels, which require extremely intense LW fluxes ($\gtrsim 1000 J_{21}$; Shang et al. (2010); Sugimura et al. (2014)). Under these flux conditions, the resulting seed abundances are more than two orders of magnitude lower than in our models (O’Brennan et al. 2025). Recent studies (Regan et al. 2020b,a; Wise et al. 2019) suggest that dynamical heating in rapidly assembling halos may substantially lower the critical LW flux required for direct collapse. However, the resulting seed masses in these scenarios tend to be significantly lower, around $\sim 10^3 M_{\odot}$. Alternative pathways for forming heavy seeds beyond the standard direct collapse path may exist—for example, rapid growth in Pop III star clusters (Vergara et al. 2025; Reinoso et al. 2025) or more exotic possibilities such as primordial black holes (Ziparo et al. 2025) or self-interacting dark matter-aided collapse (Shen et al. 2025). In any case, our results underscore the need for continued efforts to explore new mechanisms for efficiently forming heavy seeds using small-scale “resolved physics” simulations.

4.2. Modeling caveats

As we found that the $M_{\bullet} - \sigma$ evolution is substantially influenced by the relative importance of BH growth via

mergers versus accretion, it is important to acknowledge several caveats of the BRAHMA simulations that could affect this balance and must be considered when interpreting our results. One key caveat is our use of BH repositioning, which effectively causes BHs to merge instantaneously during galaxy mergers. This represents an optimistic scenario with minimal time delay between galaxy and BH mergers. Bhowmick et al. (2024c) studied the effect of merger delays on BH mass assembly and found that, for our lenient seeding models to reproduce the JWST observations, delays must be $\lesssim 750$ Myr. We are currently investigating whether such timescales are possible under more accurate BH dynamics models that include unresolved dynamical friction (Bhowmick et al., in prep).

If BH mergers turn out to be too inefficient to account for the high BH masses observed by JWST, we would need to enhance BH growth through accretion. In our simulations, Bondi-Hoyle accretion scales steeply with BH mass (M_{\bullet}^2), which makes it difficult to grow low-mass BHs efficiently. Alternative accretion models such as the α -disk model (Shakura & Sunyaev 1973), the torque-limited model (Hopkins & Quataert 2011; Anglés-Alcázar et al. 2017), and free-fall time-based models (Weinberger et al. 2025) feature shallower mass dependence and could facilitate earlier growth of our seed BHs. However, in low-mass galaxies ($\lesssim 10^9 M_{\odot}$), BH accretion is also suppressed by stellar feedback (Habouzit et al. 2017; Petersson et al. 2025). If stellar feedback evacuates gas from the BH’s vicinity, then accretion-driven growth would remain inefficient regardless of the chosen accretion prescription. In future work, we will systematically explore how the $M_{\bullet} - \sigma$ evolution and high- z BH assembly respond to alternative BH accretion models and stellar feedback implementations.

5. CONCLUSIONS

In this work, we used the recently developed BRAHMA simulations (Bhowmick et al. 2024c) to investigate whether different models for BH seed formation produce distinguishable features in BH-galaxy scaling relations, particularly the $M_{\bullet} - \sigma$ relation. These $[18 \text{ Mpc}]^3$ BRAHMA boxes inherited the galaxy formation model of its predecessor TNG, except for the addition of new BH seeding prescriptions. These prescriptions initialized heavy ($M_{\text{seed}} = 1.5 \times 10^5 M_{\odot}$) seeds within halos based on a combination of dense and metal-poor gas content, local LW intensity, gas angular momentum (spin), and environmental richness. Each of these criteria was added cumulatively—in the order listed—across successive simulations, thereby making the seeding conditions progressively more restrictive. With our simulation volume and

mass resolution ($\sim 10^5 M_{\odot}$ in gas), we were able to probe the $M_{\bullet} - \sigma$ relation in galaxies with $50 \lesssim \sigma \lesssim 200 \text{ km s}^{-1}$ at $z \sim 5$, and $50 \lesssim \sigma \lesssim 400 \text{ km s}^{-1}$ at $z = 0$.

Our main results are as follows:

1. At high redshift ($z > 2$), our BH seed models are distinguishable in the median $M_{\bullet} - \sigma$ relation across the full range of σ values probed by our simulation volume. This is because BH mass assembly is dominated by mergers within lower mass galaxies ($\lesssim 10^9 M_{\odot}$). By $z \sim 0$, however, the seed models remain differentiable only in lower-mass galaxies with $50 \text{ km s}^{-1} \lesssim \sigma \lesssim 80 \text{ km s}^{-1}$, where merger-driven growth continues to dominate. The differences between seed models become less pronounced in higher-mass ($\gtrsim 10^9 M_{\odot}$) galaxies with $\sigma \gtrsim 80 \text{ km s}^{-1}$, as BH growth is primarily fueled by gas accretion.
2. Concurrently, the seed models exert a significant influence on the redshift evolution of the median $M_{\bullet} - \sigma$ relation. While Bhowmick et al. (2025) found that the evolution of $M_{\bullet} - M_{\star}$ follows a predominantly top-down trend, the evolution of $M_{\bullet} - \sigma$ does not exhibit the same behavior. This is because the top-down evolution of $M_{\bullet} - M_{\star}$ “competes” with the bottom-up evolution of $M_{\star} - \sigma$. The relative importance of these competing effects varies across seed models, driven by differences in the rates of merger-driven BH growth. Specifically,
 - For the most lenient seed model, due to strong merger-dominated BH growth, there is no significant redshift evolution in the $M_{\bullet} - \sigma$ relation from $z \sim 5$ to $z \sim 0$. This is consistent with current JWST measurements of high- z AGN, which suggest that these BHs appear overmassive relative to the local BHs on the $M_{\bullet} - M_{\star}$ plane, but not on the $M_{\bullet} - \sigma$ plane.
 - For the more restrictive seed models, the evolution in the $M_{\bullet} - \sigma$ relation remains modest at low $\sigma < 50 \text{ km s}^{-1}$, but exhibits a steep bottom-up trend at high σ (e.g., $\sim 100 \text{ km s}^{-1}$) between $z \sim 2$ and $z \sim 0$. This is driven by the onset of gas accretion as galaxies grow to stellar masses $\gtrsim 10^9 M_{\odot}$, fueling rapid BH growth in more massive systems.
3. Finally, the scatter (IQR) in the $M_{\bullet} - \sigma$ relation at high σ (e.g., 100 km s^{-1}) is larger for the more restrictive seed models. This is because,

whereas the lenient seed models enable consistent BH growth as galaxies evolve, the restrictive seed models result in a mixed population of grown and ungrown BH seeds, leading to greater diversity in BH masses at fixed σ .

Our results highlight the potential for constraining BH seed models using the emerging population of high- z JWST AGNs and their locations on the $M_\bullet - \sigma$ and $M_\bullet - M_*$ planes. Accommodating current observations—though subject to significant uncertainties—appears to require the abundant formation of heavy ($\sim 10^5 M_\odot$) seeds that can also undergo mergers on relatively short timescales ($\lesssim 750$ Myr), as suggested by [Bhowmick et al. \(2024c\)](#). Alternatively, one could investigate mechanisms for substantially enhancing accretion-driven BH growth in low-mass galaxies ($\lesssim 10^9 M_\odot$) beyond what is seen in our simulations.

APPENDIX

A. EXPLAINING THE REDSHIFT EVOLUTION OF STELLAR MASS AT FIXED σ

In order to explain for the redshift evolution of the $M_* - \sigma$ relation seen in Fig. 7a, we plot in Fig. 8 the redshift evolution of the median half-mass radius (HMR) of subhalos at fixed stellar masses. Note that we only plot the redshift evolution for the BI box, as the evolution here is identical between seed models, even more so than the redshift evolution seen in M_* for fixed σ . We see here that the HMR tends to increase with decreasing redshift for all stellar masses.

This increase in size with decreasing redshift indicates that galaxies of a fixed mass were more compact at early times, a result that is in good agreement with current observations ([Cimatti et al. 2008](#); [Patel et al. 2017](#); [Mowla et al. 2019](#); [Clausen et al. 2025](#)) which was also reproduced in TNG ([Genel et al. 2018](#)).

This increase in HMR provides an excellent explanation for the redshift evolution seen in Fig. 7a. [Wolf et al. \(2010\)](#) show that stellar velocity dispersion and galaxy size are related as follows:

$$\sigma^2 \sim \frac{GM}{R_{\text{HM}}} \quad (\text{A1})$$

Based on this expression, we would expect the stellar mass to increase with increasing HMR for fixed σ , which is what exactly what we find.

These possibilities underscore the importance of continued efforts using small-scale “resolved physics” simulations to test the feasibility of these scenarios.

6. ACKNOWLEDGEMENTS

JK, AKB, PT, and AG acknowledge support from NSF-AST 2346977 and the NSF-Simons AI Institute for Cosmic Origins which is supported by the National Science Foundation under Cooperative Agreement 2421782 and the Simons Foundation award MPS-AI-00010515. LB acknowledges support from NSF award AST-2307171. The authors acknowledge Research Computing at The University of Virginia for providing computational resources and technical support that have contributed to the results reported within this publication. URL: <https://rc.virginia.edu>.

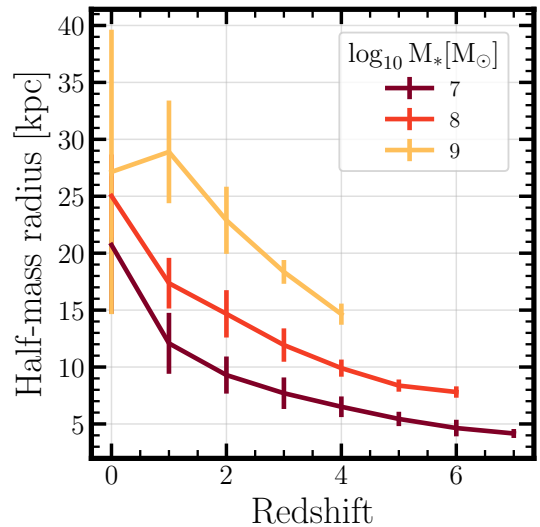


Figure 8. Redshift evolution of the half-mass radius of subhalos in the BI (most lenient model) for fixed stellar masses. The redshift evolution seen in the other three BRAHMA boxes is identical to that seen here, and so they are omitted to avoid redundancy. There is a strong increase in the size of subhalos with decreasing redshift, which explains the redshift evolution seen in Fig. 7a.

B. CONFIRMING THE EXPLANATION OF THE $M_\bullet - \sigma$ REDSHIFT EVOLUTION

In exploring the variations in the redshift evolution of the $M_\bullet - \sigma$ relation between different BH seed models, we made various approximations to calculate the different components of Eqn. 2. In this appendix, we ex-

plain and justify the various approximations made and show that they produce reasonable results. To calculate derivatives of median values with respect to decreasing redshift, we use a finite difference approximation. For component 3, we only hold M_* constant for individual finite difference calculations, (i.e. for calculating $\Delta\bar{M}_\bullet/\Delta z$ from $z = 3$ to $z = 1$ to approximate $\frac{\partial\bar{M}_\bullet}{\partial z}(z = 2)$), not across all redshifts. However, we do hold σ constant across all redshifts, as necessitated by the left-hand side (LHS) of equation 2. For component 2, we approximate $\frac{\partial\bar{M}_\bullet}{\partial M_*}|_{z,\sigma}$ to be represented by the evolution of the $M_\bullet - M_*$ relation plotted in Figure 4 (middle panel), even though the latter did not assume a fixed σ . While this effectively marginalizes $\frac{\partial\bar{M}_\bullet}{\partial M_*}|_{z,\sigma}$ over different σ values at every M_* , the approximation is nevertheless valid because of the relatively small scatter about the $M_* - \sigma$ relation (the validity of this approximation is further corroborated by our comparison of the LHS and RHS of Eqn. 2 in Fig. 9). Therefore, we perform a simple linear regression on the $M_\bullet - M_*$ data at each red-

shift for systems with BH masses greater than 5 times the seed mass¹.

To assess the validity of our approximations of Eqn. 2, we show in Fig. 9, our calculations for the LHS and RHS of this equation as a function of redshift for $\sigma = 10^{1.5}, 10^{1.75}, 10^2 \text{ km s}^{-1}$. While the LHS and RHS curves don't perfectly overlap, even our rough estimate shows that the curves follow the same trends as a function of redshift, and do tend to strongly overlap. The LHS and RHS points that don't strongly overlap are almost all within each others' 95% bootstrapped confidence intervals. The top right panel has no data because the most restrictive seed model has very few subhalos at $\sigma = 10^{1.5} \text{ km s}^{-1}$ that have been seeded with a BH. With a larger volume, this gap in the data would likely be filled, and better statistics could help alleviate some of the differences seen between our LHS and RHS curves, especially for our more restrictive seed models. Additionally, because our redshift sampling was very coarse (we only calculated finite difference approximations at $z = 1, 2, 3, 4, 5, 6$), we should expect that our finite difference approximations do not perfectly capture the true derivatives.

REFERENCES

- Abadi, M. G., Navarro, J. F., Steinmetz, M., & Eke, V. R. 2003, *ApJ*, 591, 499, doi: [10.1086/375512](https://doi.org/10.1086/375512)
- Agarwal, B., Davis, A. J., Khochfar, S., Natarajan, P., & Dunlop, J. S. 2013, *MNRAS*, 432, 3438, doi: [10.1093/mnras/stt696](https://doi.org/10.1093/mnras/stt696)
- Akins, H. B., Casey, C. M., Allen, N., et al. 2023, *ApJ*, 956, 61, doi: [10.3847/1538-4357/acef21](https://doi.org/10.3847/1538-4357/acef21)
- Akins, H. B., Casey, C. M., Lambrides, E., et al. 2024, arXiv e-prints, arXiv:2406.10341, doi: [10.48550/arXiv.2406.10341](https://doi.org/10.48550/arXiv.2406.10341)
- Ananna, T. T., Bogdán, Á., Kovács, O. E., Natarajan, P., & Hickox, R. C. 2024, *ApJL*, 969, L18, doi: [10.3847/2041-8213/ad5669](https://doi.org/10.3847/2041-8213/ad5669)
- Anglés-Alcázar, D., Davé, R., Faucher-Giguère, C.-A., Özel, F., & Hopkins, P. F. 2017, *MNRAS*, 464, 2840, doi: [10.1093/mnras/stw2565](https://doi.org/10.1093/mnras/stw2565)
- Arca Sedda, M., Kamlah, A. W. H., Spurzem, R., et al. 2023, *MNRAS*, 526, 429, doi: [10.1093/mnras/stad2292](https://doi.org/10.1093/mnras/stad2292)
- Barnes, J., & Hut, P. 1986, *Nature*, 324, 446, doi: [10.1038/324446a0](https://doi.org/10.1038/324446a0)
- Bhowmick, A. K., Blecha, L., Torrey, P., et al. 2022a, *MNRAS*, 510, 177, doi: [10.1093/mnras/stab3439](https://doi.org/10.1093/mnras/stab3439)
- . 2024a, *MNRAS*, 529, 3768, doi: [10.1093/mnras/stae780](https://doi.org/10.1093/mnras/stae780)
- . 2021, *MNRAS*, 507, 2012, doi: [10.1093/mnras/stab2204](https://doi.org/10.1093/mnras/stab2204)
- Bhowmick, A. K., Blecha, L., Ni, Y., et al. 2022b, *MNRAS*, 516, 138, doi: [10.1093/mnras/stac2238](https://doi.org/10.1093/mnras/stac2238)
- Bhowmick, A. K., Blecha, L., Torrey, P., et al. 2024b, *MNRAS*, 531, 4311, doi: [10.1093/mnras/stae1386](https://doi.org/10.1093/mnras/stae1386)
- . 2024c, *MNRAS*, 533, 1907, doi: [10.1093/mnras/stae1819](https://doi.org/10.1093/mnras/stae1819)
- . 2025, *MNRAS*, 538, 518, doi: [10.1093/mnras/staf269](https://doi.org/10.1093/mnras/staf269)
- Bogdán, Á., Goulding, A. D., Natarajan, P., et al. 2024, *Nature Astronomy*, 8, 126, doi: [10.1038/s41550-023-02111-9](https://doi.org/10.1038/s41550-023-02111-9)
- Bondi, H. 1952, *MNRAS*, 112, 195, doi: [10.1093/mnras/112.2.195](https://doi.org/10.1093/mnras/112.2.195)
- Bondi, H., & Hoyle, F. 1944, *MNRAS*, 104, 273, doi: [10.1093/mnras/104.5.273](https://doi.org/10.1093/mnras/104.5.273)
- Bottrell, C., Torrey, P., Simard, L., & Ellison, S. L. 2017, *MNRAS*, 467, 2879, doi: [10.1093/mnras/stx276](https://doi.org/10.1093/mnras/stx276)
- Chabrier, G. 2003, *PASP*, 115, 763, doi: [10.1086/376392](https://doi.org/10.1086/376392)
- Cimatti, A., Cassata, P., Pozzetti, L., et al. 2008, *A&A*, 482, 21, doi: [10.1051/0004-6361:20078739](https://doi.org/10.1051/0004-6361:20078739)

¹ This mass cut was applied to mitigate the effect of the artificial flattening of the $M_\bullet - M_*$ relation for low-mass systems in our more restrictive models, which is a consequence of our fixed initial seed mass (see column 2 of Fig. 4). We thus calculate the slope for only those BHs which are growing.

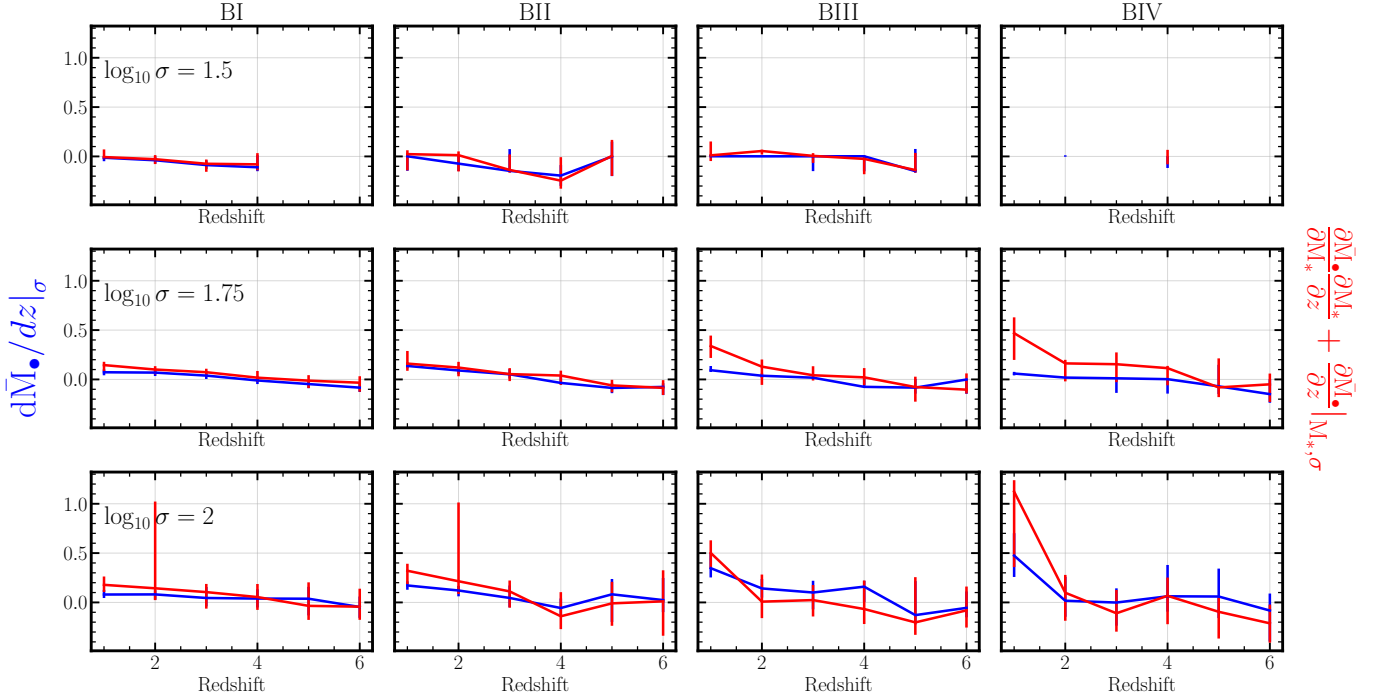


Figure 9. Approximated trends of the LHS (blue) and RHS (red) of Eqn. 2 as a function of redshift for $\sigma = 10^{1.5}, 10^{1.75}, 10^2$ km s^{-1} . Even with the various approximations we made, the trends clearly follow the same redshift evolution, and show that a combination of the slope of the $M_{\bullet} - M_{\star}$ relation, the stellar mass at constant σ redshift evolution, and the explicit BH mass redshift dependence do a good job at explaining the redshift evolution in the $M_{\bullet} - \sigma$ relation.

Clausen, M., Momcheva, I., Whitaker, K. E., et al. 2025, arXiv e-prints, arXiv:2501.04788, doi: [10.48550/arXiv.2501.04788](https://doi.org/10.48550/arXiv.2501.04788)

Davis, M., Efstathiou, G., Frenk, C. S., & White, S. D. M. 1985, ApJ, 292, 371, doi: [10.1086/163168](https://doi.org/10.1086/163168)

Di Matteo, T., Springel, V., & Hernquist, L. 2005, Nature, 433, 604, doi: [10.1038/nature03335](https://doi.org/10.1038/nature03335)

Du, M., Ho, L. C., Debattista, V. P., et al. 2020, ApJ, 895, 139, doi: [10.3847/1538-4357/ab8fa8](https://doi.org/10.3847/1538-4357/ab8fa8)

Du, M., Ho, L. C., Zhao, D., et al. 2019, ApJ, 884, 129, doi: [10.3847/1538-4357/ab43cc](https://doi.org/10.3847/1538-4357/ab43cc)

Dunn, G., Bellovary, J., Holley-Bockelmann, K., Christensen, C., & Quinn, T. 2018, ApJ, 861, 39, doi: [10.3847/1538-4357/aac7c2](https://doi.org/10.3847/1538-4357/aac7c2)

Evans, A. E., Blecha, L., & Bhowmick, A. K. 2025, MNRAS, 536, 2783, doi: [10.1093/mnras/stae2735](https://doi.org/10.1093/mnras/stae2735)

Ferrarese, L., & Merritt, D. 2000, ApJL, 539, L9, doi: [10.1086/312838](https://doi.org/10.1086/312838)

Fragione, G., Kocsis, B., Rasio, F. A., & Silk, J. 2022, ApJ, 927, 231, doi: [10.3847/1538-4357/ac5026](https://doi.org/10.3847/1538-4357/ac5026)

Furtak, L. J., Labbé, I., Zitrin, A., et al. 2024, Nature, 628, 57, doi: [10.1038/s41586-024-07184-8](https://doi.org/10.1038/s41586-024-07184-8)

Gebhardt, K., Bender, R., Bower, G., et al. 2000, ApJL, 539, L13, doi: [10.1086/312840](https://doi.org/10.1086/312840)

Genel, S., Nelson, D., Pillepich, A., et al. 2018, MNRAS, 474, 3976, doi: [10.1093/mnras/stx3078](https://doi.org/10.1093/mnras/stx3078)

Greene, J. E., Labbe, I., Goulding, A. D., et al. 2024, ApJ, 964, 39, doi: [10.3847/1538-4357/ad1e5f](https://doi.org/10.3847/1538-4357/ad1e5f)

Habouzit, M., Volonteri, M., & Dubois, Y. 2017, MNRAS, 468, 3935, doi: [10.1093/mnras/stx666](https://doi.org/10.1093/mnras/stx666)

Habouzit, M., Genel, S., Somerville, R. S., et al. 2019, MNRAS, 484, 4413, doi: [10.1093/mnras/stz102](https://doi.org/10.1093/mnras/stz102)

Hahn, O., & Abel, T. 2011, MNRAS, 415, 2101, doi: [10.1111/j.1365-2966.2011.18820.x](https://doi.org/10.1111/j.1365-2966.2011.18820.x)

Harikane, Y., Zhang, Y., Nakajima, K., et al. 2023, ApJ, 959, 39, doi: [10.3847/1538-4357/ad029e](https://doi.org/10.3847/1538-4357/ad029e)

Heger, A., Müller, B., & Mandel, I. 2023, arXiv e-prints, arXiv:2304.09350, doi: [10.48550/arXiv.2304.09350](https://doi.org/10.48550/arXiv.2304.09350)

Ho, L. C. 2008, ARA&A, 46, 475,

doi: [10.1146/annurev.astro.45.051806.110546](https://doi.org/10.1146/annurev.astro.45.051806.110546)

Hopkins, P. F., & Quataert, E. 2011, MNRAS, 415, 1027, doi: [10.1111/j.1365-2966.2011.18542.x](https://doi.org/10.1111/j.1365-2966.2011.18542.x)

Huang, K.-W., Di Matteo, T., Bhowmick, A. K., Feng, Y., & Ma, C.-P. 2018, MNRAS, 478, 5063, doi: [10.1093/mnras/sty1329](https://doi.org/10.1093/mnras/sty1329)

Inayoshi, K., Visbal, E., & Haiman, Z. 2020, ARA&A, 58, 27, doi: [10.1146/annurev-astro-120419-014455](https://doi.org/10.1146/annurev-astro-120419-014455)

Jeon, J., Liu, B., Bromm, V., & Finkelstein, S. L. 2023, MNRAS, 524, 176, doi: [10.1093/mnras/stad1877](https://doi.org/10.1093/mnras/stad1877)

- Juodžbalis, I., Maiolino, R., Baker, W. M., et al. 2025, arXiv e-prints, arXiv:2504.03551, doi: [10.48550/arXiv.2504.03551](https://doi.org/10.48550/arXiv.2504.03551)
- Katz, N., Weinberg, D. H., & Hernquist, L. 1996, ApJS, 105, 19, doi: [10.1086/192305](https://doi.org/10.1086/192305)
- Kido, D., Ioka, K., Hotokezaka, K., Inayoshi, K., & Irwin, C. M. 2025, arXiv e-prints, arXiv:2505.06965. <https://arxiv.org/abs/2505.06965>
- Klessen, R. S., & Glover, S. C. O. 2023, ARA&A, 61, 65, doi: [10.1146/annurev-astro-071221-053453](https://doi.org/10.1146/annurev-astro-071221-053453)
- Kokorev, V., Caputi, K. I., Greene, J. E., et al. 2024, ApJ, 968, 38, doi: [10.3847/1538-4357/ad4265](https://doi.org/10.3847/1538-4357/ad4265)
- Kormendy, J., & Ho, L. C. 2013, ARA&A, 51, 511, doi: [10.1146/annurev-astro-082708-101811](https://doi.org/10.1146/annurev-astro-082708-101811)
- Kormendy, J., & Richstone, D. 1995, ARA&A, 33, 581, doi: [10.1146/annurev.aa.33.090195.003053](https://doi.org/10.1146/annurev.aa.33.090195.003053)
- Kovács, O. E., Bogdán, Á., Natarajan, P., et al. 2024, ApJL, 965, L21, doi: [10.3847/2041-8213/ad391f](https://doi.org/10.3847/2041-8213/ad391f)
- Laplace, E., Schneider, F. R. N., & Podsiadlowski, P. 2025, A&A, 695, A71, doi: [10.1051/0004-6361/202451077](https://doi.org/10.1051/0004-6361/202451077)
- Lin, X., Wang, F., Fan, X., et al. 2024, ApJ, 974, 147, doi: [10.3847/1538-4357/ad6565](https://doi.org/10.3847/1538-4357/ad6565)
- Lodato, G., & Natarajan, P. 2006, MNRAS, 371, 1813, doi: [10.1111/j.1365-2966.2006.10801.x](https://doi.org/10.1111/j.1365-2966.2006.10801.x)
- Luo, Y., Shlosman, I., Nagamine, K., & Fang, T. 2020, MNRAS, 492, 4917, doi: [10.1093/mnras/staa153](https://doi.org/10.1093/mnras/staa153)
- Magorrian, J., Tremaine, S., Richstone, D., et al. 1998, AJ, 115, 2285, doi: [10.1086/300353](https://doi.org/10.1086/300353)
- Maiolino, R., Scholtz, J., Witstok, J., et al. 2024a, Nature, 627, 59, doi: [10.1038/s41586-024-07052-5](https://doi.org/10.1038/s41586-024-07052-5)
- Maiolino, R., Scholtz, J., Curtis-Lake, E., et al. 2024b, A&A, 691, A145, doi: [10.1051/0004-6361/202347640](https://doi.org/10.1051/0004-6361/202347640)
- Marconi, A., & Hunt, L. K. 2003, ApJL, 589, L21, doi: [10.1086/375804](https://doi.org/10.1086/375804)
- Marinacci, F., Vogelsberger, M., Pakmor, R., et al. 2018, MNRAS, 480, 5113, doi: [10.1093/mnras/sty2206](https://doi.org/10.1093/mnras/sty2206)
- Milosavljević, M., Couch, S. M., & Bromm, V. 2009, ApJL, 696, L146, doi: [10.1088/0004-637X/696/2/L146](https://doi.org/10.1088/0004-637X/696/2/L146)
- Mowla, L. A., van Dokkum, P., Brammer, G. B., et al. 2019, ApJ, 880, 57, doi: [10.3847/1538-4357/ab290a](https://doi.org/10.3847/1538-4357/ab290a)
- Naidu, R. P., Matthee, J., Katz, H., et al. 2025, arXiv e-prints, arXiv:2503.16596, doi: [10.48550/arXiv.2503.16596](https://doi.org/10.48550/arXiv.2503.16596)
- Naiman, J. P., Pillepich, A., Springel, V., et al. 2018, MNRAS, 477, 1206, doi: [10.1093/mnras/sty618](https://doi.org/10.1093/mnras/sty618)
- Natarajan, P., Pacucci, F., Ferrara, A., et al. 2017, ApJ, 838, 117, doi: [10.3847/1538-4357/aa6330](https://doi.org/10.3847/1538-4357/aa6330)
- Natarajan, P., Pacucci, F., Ricarte, A., et al. 2024, ApJL, 960, L1, doi: [10.3847/2041-8213/ad0e76](https://doi.org/10.3847/2041-8213/ad0e76)
- Nelson, D., Pillepich, A., Springel, V., et al. 2018, MNRAS, 475, 624, doi: [10.1093/mnras/stx3040](https://doi.org/10.1093/mnras/stx3040)
- O’Brennan, H., Regan, J. A., Brennan, J., et al. 2025, arXiv e-prints, arXiv:2502.00574, doi: [10.48550/arXiv.2502.00574](https://doi.org/10.48550/arXiv.2502.00574)
- Pacucci, F., & Loeb, A. 2024, ApJ, 964, 154, doi: [10.3847/1538-4357/ad3044](https://doi.org/10.3847/1538-4357/ad3044)
- Pacucci, F., Nguyen, B., Carniani, S., Maiolino, R., & Fan, X. 2023, ApJL, 957, L3, doi: [10.3847/2041-8213/ad0158](https://doi.org/10.3847/2041-8213/ad0158)
- Pakmor, R., Bauer, A., & Springel, V. 2011, MNRAS, 418, 1392, doi: [10.1111/j.1365-2966.2011.19591.x](https://doi.org/10.1111/j.1365-2966.2011.19591.x)
- Pakmor, R., Pfrommer, C., Simpson, C. M., Kannan, R., & Springel, V. 2016, MNRAS, 462, 2603, doi: [10.1093/mnras/stw1761](https://doi.org/10.1093/mnras/stw1761)
- Patel, S. G., Hong, Y. X., Quadri, R. F., Holden, B. P., & Williams, R. J. 2017, ApJ, 839, 127, doi: [10.3847/1538-4357/aa6bf4](https://doi.org/10.3847/1538-4357/aa6bf4)
- Pérez-González, P. G., Barro, G., Rieke, G. H., et al. 2024, ApJ, 968, 4, doi: [10.3847/1538-4357/ad38bb](https://doi.org/10.3847/1538-4357/ad38bb)
- Petersson, J., Hirschmann, M., Tress, R. G., et al. 2025, arXiv e-prints, arXiv:2504.08035, doi: [10.48550/arXiv.2504.08035](https://doi.org/10.48550/arXiv.2504.08035)
- Pezzulli, E., Valiante, R., & Schneider, R. 2016, MNRAS, 458, 3047, doi: [10.1093/mnras/stw505](https://doi.org/10.1093/mnras/stw505)
- Pillepich, A., Springel, V., Nelson, D., et al. 2018a, MNRAS, 473, 4077, doi: [10.1093/mnras/stx2656](https://doi.org/10.1093/mnras/stx2656)
- Pillepich, A., Nelson, D., Hernquist, L., et al. 2018b, MNRAS, 475, 648, doi: [10.1093/mnras/stx3112](https://doi.org/10.1093/mnras/stx3112)
- Planck Collaboration, Ade, P. A. R., Aghanim, N., et al. 2016, A&A, 594, A13, doi: [10.1051/0004-6361/201525830](https://doi.org/10.1051/0004-6361/201525830)
- Portegies Zwart, S. F., & McMillan, S. L. W. 2002, ApJ, 576, 899, doi: [10.1086/341798](https://doi.org/10.1086/341798)
- Ramos Padilla, A. F., Ashby, M. L. N., Smith, H. A., et al. 2020, MNRAS, 499, 4325, doi: [10.1093/mnras/staa2813](https://doi.org/10.1093/mnras/staa2813)
- Regan, J., & Volonteri, M. 2024, The Open Journal of Astrophysics, 7, 72, doi: [10.33232/001c.123239](https://doi.org/10.33232/001c.123239)
- Regan, J. A., Wise, J. H., O’Shea, B. W., & Norman, M. L. 2020a, MNRAS, 492, 3021, doi: [10.1093/mnras/staa035](https://doi.org/10.1093/mnras/staa035)
- Regan, J. A., Wise, J. H., Woods, T. E., et al. 2020b, The Open Journal of Astrophysics, 3, 15, doi: [10.21105/astro.2008.08090](https://doi.org/10.21105/astro.2008.08090)
- Reines, A. E., & Volonteri, M. 2015, ApJ, 813, 82, doi: [10.1088/0004-637X/813/2/82](https://doi.org/10.1088/0004-637X/813/2/82)
- Reinoso, B., Klessen, R. S., Schleicher, D., Glover, S. C. O., & Solar, P. 2023, MNRAS, 521, 3553, doi: [10.1093/mnras/stad790](https://doi.org/10.1093/mnras/stad790)
- Reinoso, B., Latif, M. A., & Schleicher, D. R. G. 2025, arXiv e-prints, arXiv:2503.20415, doi: [10.48550/arXiv.2503.20415](https://doi.org/10.48550/arXiv.2503.20415)

- Rusakov, V., Watson, D., Nikopoulos, G. P., et al. 2025, arXiv e-prints, arXiv:2503.16595, doi: [10.48550/arXiv.2503.16595](https://doi.org/10.48550/arXiv.2503.16595)
- Scoggins, M. T., & Haiman, Z. 2024, *Monthly Notices of the Royal Astronomical Society*, 531, 4584, doi: [10.1093/mnras/stae1449](https://doi.org/10.1093/mnras/stae1449)
- Scoggins, M. T., Haiman, Z., & Wise, J. H. 2023, *MNRAS*, 519, 2155, doi: [10.1093/mnras/stac3715](https://doi.org/10.1093/mnras/stac3715)
- Shakura, N. I., & Sunyaev, R. A. 1973, *A&A*, 24, 337
- Shang, C., Bryan, G. L., & Haiman, Z. 2010, *MNRAS*, 402, 1249, doi: [10.1111/j.1365-2966.2009.15960.x](https://doi.org/10.1111/j.1365-2966.2009.15960.x)
- Shapiro, S. L., & Teukolsky, S. A. 1983, *Black holes, white dwarfs and neutron stars. The physics of compact objects*, doi: [10.1002/9783527617661](https://doi.org/10.1002/9783527617661)
- Shen, T., Shen, X., Xiao, H., Vogelsberger, M., & Jiang, F. 2025, arXiv e-prints, arXiv:2504.00075, doi: [10.48550/arXiv.2504.00075](https://doi.org/10.48550/arXiv.2504.00075)
- Smith, B. D., Regan, J. A., Downes, T. P., et al. 2018, *MNRAS*, 480, 3762, doi: [10.1093/mnras/sty2103](https://doi.org/10.1093/mnras/sty2103)
- Soltan, A. 1982, *MNRAS*, 200, 115, doi: [10.1093/mnras/200.1.115](https://doi.org/10.1093/mnras/200.1.115)
- Spinoso, D., Bonoli, S., Valiante, R., Schneider, R., & Izquierdo-Villalba, D. 2023, *MNRAS*, 518, 4672, doi: [10.1093/mnras/stac3169](https://doi.org/10.1093/mnras/stac3169)
- Springel, V. 2010, *MNRAS*, 401, 791, doi: [10.1111/j.1365-2966.2009.15715.x](https://doi.org/10.1111/j.1365-2966.2009.15715.x)
- Springel, V., & Hernquist, L. 2003, *MNRAS*, 339, 289, doi: [10.1046/j.1365-8711.2003.06206.x](https://doi.org/10.1046/j.1365-8711.2003.06206.x)
- Springel, V., White, S. D. M., Tormen, G., & Kauffmann, G. 2001, *MNRAS*, 328, 726, doi: [10.1046/j.1365-8711.2001.04912.x](https://doi.org/10.1046/j.1365-8711.2001.04912.x)
- Springel, V., Pakmor, R., Pillepich, A., et al. 2018, *MNRAS*, 475, 676, doi: [10.1093/mnras/stx3304](https://doi.org/10.1093/mnras/stx3304)
- Stark, D. P., Topping, M. W., Endsley, R., & Tang, M. 2025, arXiv e-prints, arXiv:2501.17078, doi: [10.48550/arXiv.2501.17078](https://doi.org/10.48550/arXiv.2501.17078)
- Sugimura, K., Omukai, K., & Inoue, A. K. 2014, *MNRAS*, 445, 544, doi: [10.1093/mnras/stu1778](https://doi.org/10.1093/mnras/stu1778)
- Sun, Y., Rieke, G. H., Lyu, J., et al. 2025, arXiv e-prints, arXiv:2503.03675, doi: [10.48550/arXiv.2503.03675](https://doi.org/10.48550/arXiv.2503.03675)
- Tanaka, T., & Haiman, Z. 2009, *ApJ*, 696, 1798, doi: [10.1088/0004-637X/696/2/1798](https://doi.org/10.1088/0004-637X/696/2/1798)
- Terrazas, B. A., Bell, E. F., Pillepich, A., et al. 2020, *MNRAS*, 493, 1888, doi: [10.1093/mnras/staa374](https://doi.org/10.1093/mnras/staa374)
- Toomre, A. 1964, *ApJ*, 139, 1217, doi: [10.1086/147861](https://doi.org/10.1086/147861)
- Torrey, P., Vogelsberger, M., Genel, S., et al. 2014, *MNRAS*, 438, 1985, doi: [10.1093/mnras/stt2295](https://doi.org/10.1093/mnras/stt2295)
- Valiante, R., Schneider, R., Volonteri, M., & Omukai, K. 2016, *MNRAS*, 457, 3356, doi: [10.1093/mnras/stw225](https://doi.org/10.1093/mnras/stw225)
- Vergara, M. C., Askar, A., Kamlah, A. W. H., et al. 2025, arXiv e-prints, arXiv:2505.07491, doi: [10.48550/arXiv.2505.07491](https://doi.org/10.48550/arXiv.2505.07491)
- Visbal, E., & Haiman, Z. 2018, *ApJL*, 865, L9, doi: [10.3847/2041-8213/aadf3a](https://doi.org/10.3847/2041-8213/aadf3a)
- Vogelsberger, M., Genel, S., Sijacki, D., et al. 2013, *MNRAS*, 436, 3031, doi: [10.1093/mnras/stt1789](https://doi.org/10.1093/mnras/stt1789)
- Volonteri, M. 2010, *A&A Rv*, 18, 279, doi: [10.1007/s00159-010-0029-x](https://doi.org/10.1007/s00159-010-0029-x)
- Volonteri, M., & Natarajan, P. 2009, *MNRAS*, 400, 1911, doi: [10.1111/j.1365-2966.2009.15577.x](https://doi.org/10.1111/j.1365-2966.2009.15577.x)
- Volonteri, M., & Rees, M. J. 2005, *ApJ*, 633, 624, doi: [10.1086/466521](https://doi.org/10.1086/466521)
- Weinberger, R., Bhowmick, A., Blecha, L., et al. 2025, arXiv e-prints, arXiv:2502.13241, doi: [10.48550/arXiv.2502.13241](https://doi.org/10.48550/arXiv.2502.13241)
- Weinberger, R., Springel, V., & Pakmor, R. 2020, *ApJS*, 248, 32, doi: [10.3847/1538-4365/ab908c](https://doi.org/10.3847/1538-4365/ab908c)
- Weinberger, R., Springel, V., Hernquist, L., et al. 2017, *MNRAS*, 465, 3291, doi: [10.1093/mnras/stw2944](https://doi.org/10.1093/mnras/stw2944)
- Weinberger, R., Springel, V., Pakmor, R., et al. 2018, *MNRAS*, 479, 4056, doi: [10.1093/mnras/sty1733](https://doi.org/10.1093/mnras/sty1733)
- Wiersma, R. P. C., Schaye, J., & Smith, B. D. 2009, *MNRAS*, 393, 99, doi: [10.1111/j.1365-2966.2008.14191.x](https://doi.org/10.1111/j.1365-2966.2008.14191.x)
- Williams, C. C., Alberts, S., Ji, Z., et al. 2024, *ApJ*, 968, 34, doi: [10.3847/1538-4357/ad3f17](https://doi.org/10.3847/1538-4357/ad3f17)
- Wise, J. H., Regan, J. A., O'Shea, B. W., et al. 2019, *Nature*, 566, 85, doi: [10.1038/s41586-019-0873-4](https://doi.org/10.1038/s41586-019-0873-4)
- Wolf, J., Martinez, G. D., Bullock, J. S., et al. 2010, *MNRAS*, 406, 1220, doi: [10.1111/j.1365-2966.2010.16753.x](https://doi.org/10.1111/j.1365-2966.2010.16753.x)
- Ziparo, F., Gallerani, S., & Ferrara, A. 2025, *JCAP*, 2025, 040, doi: [10.1088/1475-7516/2025/04/040](https://doi.org/10.1088/1475-7516/2025/04/040)